Chapter 2. The Energy balance, hydrological and carbon cycles

2.1 The Earth's energy budget

2.1.1 The heat balance at the top of the atmosphere: a global view

Nearly all the energy entering the **climate system** comes from the Sun in the form of **electromagnetic radiation**. Additional sources are present, such as geothermal heating for instance, but their contribution is so small that their influence can safely be neglected. At the top of the Earth's atmosphere, a surface at the mean Earth-Sun distance perpendicular to the rays receives about 1368 W/m^2 (see also Figure 5.27). This is often called the **Total Solar Irradiance (TSI)** or **solar constant** S_0. A bit less than half of this energy comes in the form of radiation in the visible part of the **electromagnetic spectrum**, the remaining part being mainly in the near infrared, with a smaller contribution from the ultraviolet part of the spectrum (Fig. 2.1).
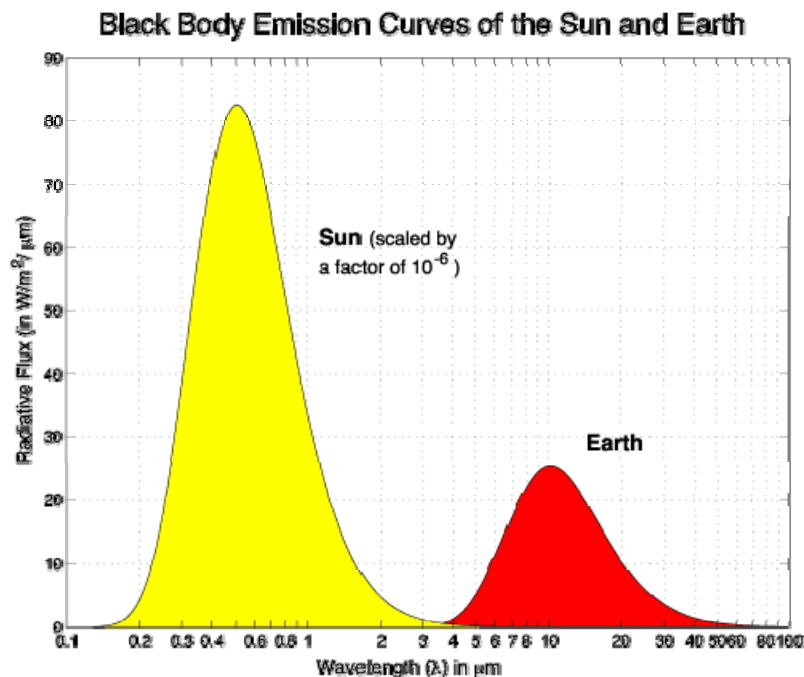

Figure 2.1: **Spectrum** of the energy received from the Sun and emitted by the Earth at the top of the atmosphere. Figure from Y. Kushnir available at http://www.ldeo.columbia.edu/~kushnir/MPA-ENVP/Climate/lectures/energy/. Reproduced with permission.

On average, the total amount of incoming solar energy outside the Earth's atmosphere (Fig 2.2) is the **solar constant** times the cross-sectional surface (i.e., the surface that intercepts the solar rays, which corresponds to a surface πR^2 where R is the Earth's radius of 6371 km^2). For simplicity and because it is a reasonable approximation, we will neglect the thickness of the atmosphere compared to the Earth's radius in our computations of distances or surfaces. Some of this incoming flux is reflected straight back to space by the atmosphere, the clouds and the Earth's surface. The fraction of the radiation that is reflected is called the **albedo** of the Earth or planetary albedo (α_p). In present-day conditions, it has a value of about 0.3.
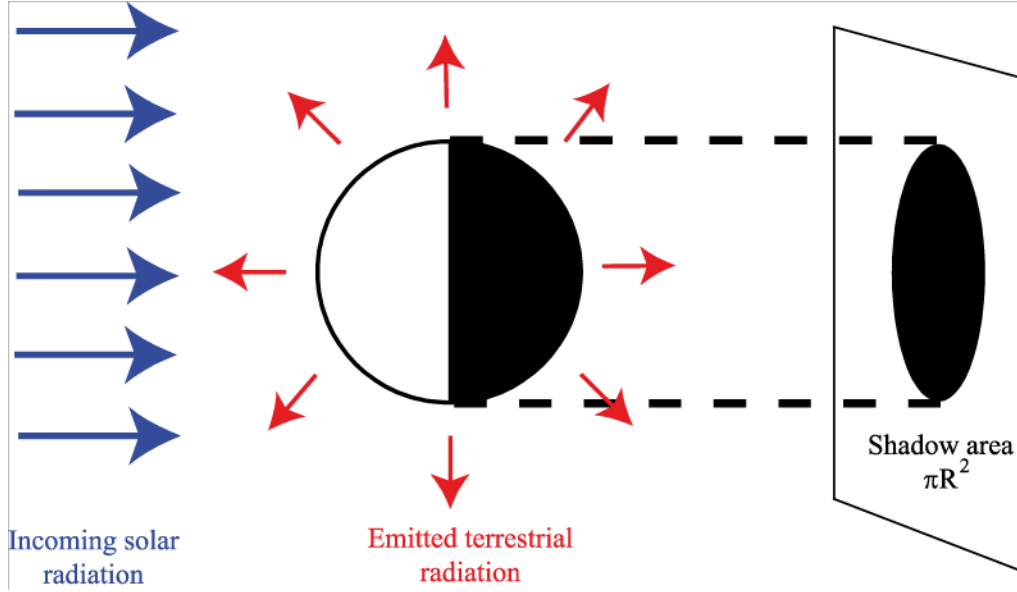
Figure 2.2: Heat absorbed and emitted by the Earth.

In order to achieve a heat balance, the heat flux coming from the Sun must be compensated for by an equivalent heat loss. If this were not true, the Earth's temperature would rapidly rise or fall. At the Earth's temperature, following **Wien's Law**, this is achieved by radiating energy in the infrared part of the electromagnetic spectrum. As the radiations emitted by the Earth have a much longer wavelength than those received from the Sun, they are often termed **longwave radiation** while those from the Sun are called **shortwave radiation**. Treating the Earth as a **black body**, the total amount of energy that is emitted by a 1 m^2 surface ($A\uparrow$) can be computed by **Stefan-Boltzmann's** law:

$$A\uparrow = \sigma T_e^4 \qquad (2.1)$$

where σ is the Stefan Boltzmann constant (σ=5.67 10^{-8} W m^{-2} K^{-4}). This equation defines T_e, effective emission temperature of the Earth. The Earth emits energy in the directions, so the total amount of energy emitted by the Earth is $A\uparrow$ times the surface of the Earth, $4\pi R^2$. To achieve equilibrium, we must thus have (Fig. 2.3):

Absorbed solar radiation = emitted terrestrial radiation

$$\pi R^2 \left(1-\alpha_p\right) S_0 = 4\pi R^2 \sigma T_e^4 \qquad (2.2)$$

This leads to

$$\frac{1}{4}\left(1-\alpha_p\right) S_0 = \sigma T_e^4 \qquad (2.3)$$

and finally to

$$T_e = \left(\frac{1}{4\sigma}\left(1-\alpha_p\right) S_0\right)^{1/4} \qquad (2.4)$$

This corresponds to T_e=255 K (=-18°C). Note that we can interpret Eq. (2.3) as the mean balance between the emitted terrestrial radiation and the absorbed solar flux for 1 m^2 of the Earth's surface. As shown above, the factor 1/4 arises from the spherical geometry of the Earth, because only part of the Earth's surface receives solar radiation directly.
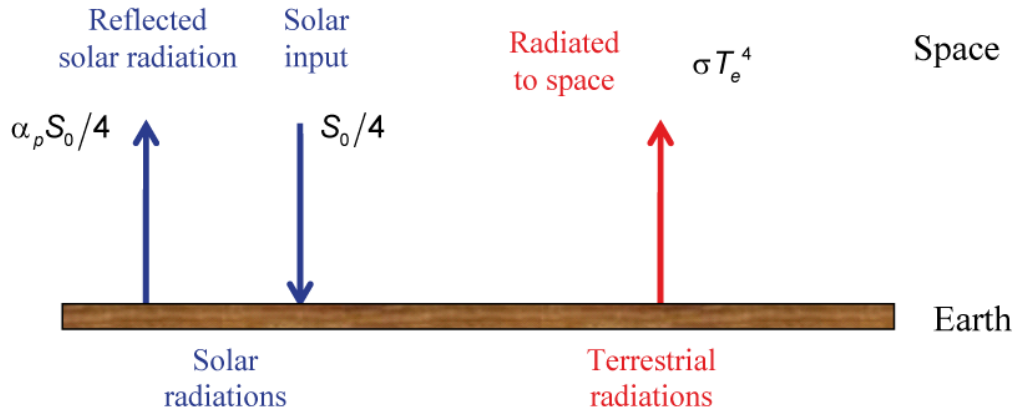
Figure 2.3: Simple heat balance of the Earth (assuming it behaves like a perfect blackbody).

The temperature T_e is not a real temperature that could be measured somewhere on Earth. It is only the black body temperature required to balance the solar energy input. It can also be interpreted as the temperature that would occur on the Earth's surface if it were a perfect black body, there were no atmosphere, and the temperature was the same at every point.

2.1.2 The greenhouse effect

The atmosphere is nearly transparent to visible light, absorbing about 20% of the incoming solar radiation. As a consequence, the majority of the absorption takes place at Earth's surface (see section 2.1.6). On the other hand, the atmosphere is almost opaque across most of the infrared part of the **electromagnetic spectrum**. This is related to the radiative properties of some minor constituents of the atmosphere, especially water vapour, carbon dioxide, methane and ozone. Those gases constitute only a small fraction of the atmospheric composition, while the two dominant components (molecular nitrogen and oxygen, see section 1.2) play nearly no part in this opacity. Nevertheless, a significant fraction of the energy emitted by the Earth's surface is absorbed by the atmosphere and re-emitted, significantly increasing the temperature of the system.

In a garden greenhouse, panes of glass are transparent to visible light but opaque to infra-red radiation, 'trapping' part of the energy emitted by the surface and resulting in a warming of the air. By analogy, the alteration of the energy budget by some minor atmospheric constituents described above is called the greenhouse effect and those minor constituents the greenhouse gases. However, the climate system is much more complex than a greenhouse and in a garden greenhouse a significant fraction of the warming is related to the reduction of the turbulent heat exchanges with atmosphere, not in the modification of the radiative fluxes. The analogy should be used with caution.

The greenhouse effect can be illustrated by a very simple model in which the atmosphere is represented by a single homogenous layer of temperature T_a, totally transparent to the solar radiation and totally opaque to the infrared radiations emitted by the Earth's surface (Fig. 2.4). Because of this opacity of the atmosphere to surface radiation, all the energy radiated to space is from the atmosphere. Using Equation 2.3, the balance at the top of the atmosphere is thus:

$$\sigma T_a^4 = \frac{1}{4}\left(1 - \alpha_p\right)S_0 = \sigma T_e^4 \qquad (2.5)$$

In this simple model, T_a is thus equal to T_e, the effective emission temperature of the Earth. At the Earth's surface, the balance between the energy emitted by the surface, and the incoming solar fluxes, and the infra-red flux coming from the atmosphere gives:

$$\sigma T_s^4 = \frac{1}{4}(1-\alpha_p)S_0 + \sigma T_a^4 \qquad (2.6)$$

Combining (2.5) and (2.6) leads to

$$\sigma T_s^4 = \sigma T_e^4 + \sigma T_e^4 \qquad (2.7)$$

and

$$T_s = 2^{\frac{1}{4}}T_e = 1.19 T_e \qquad (2.8)$$

Because of the greenhouse effect, the surface temperature is thus much higher than T_e, reaching 303K (30°C) in this example. This temperature is actually higher that the observed mean surface temperature of 288K (15°C) because of some crude approximations in this simple model.
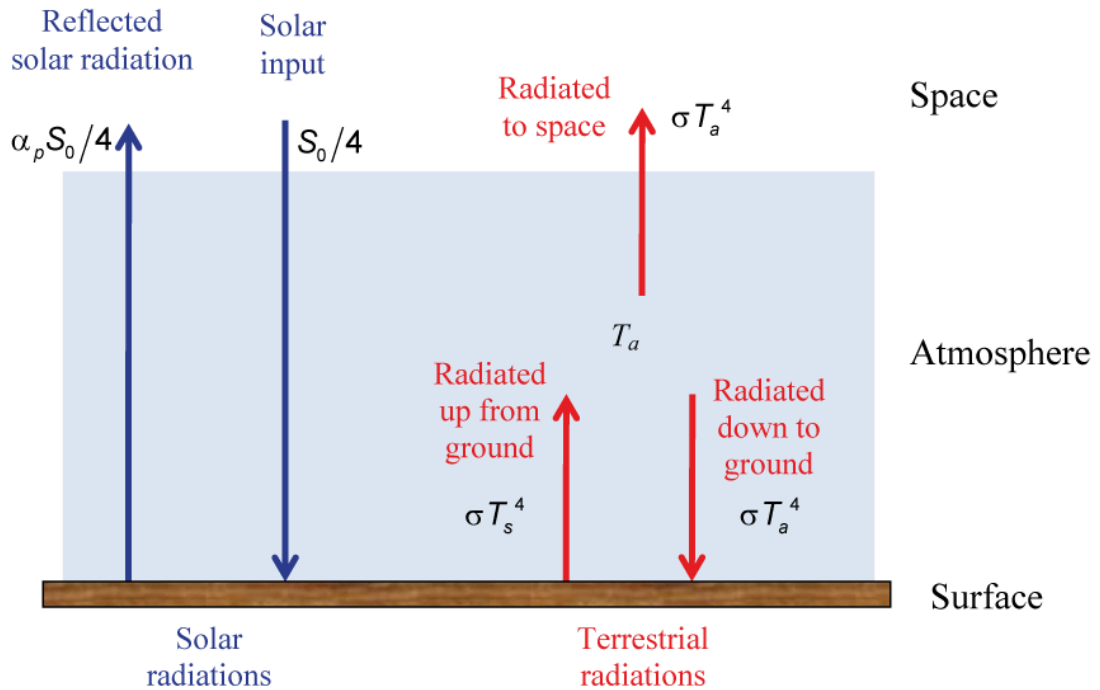

Figure 2.4: Heat balance of the Earth with an atmosphere represented by a single layer which is totally transparent to solar radiation and opaque to infrared radiations (modified from Marshall and Plumb, 2007).

We can improve our model by taking into account the fact that the atmosphere is not a perfect blackbody (Fig. 2.5). Using the emissivity of an object (ε) (which is defined as the ratio of energy radiated by this object to energy radiated by a black body at the same temperature), we can write the balance at the surface as:

$$\sigma T_s^{\,4} = \frac{1}{4}(1-\alpha_p)S_0 + \varepsilon\sigma T_a^{\,4} \qquad (2.9)$$

The emissivity is also equal to the fraction of the radiation that is absorbed by the object. The fraction being transmitted through the object is thus equal to $(1-\varepsilon)$ and the balance at the top of the atmosphere is:

$$\frac{1}{4}\left(1-\alpha_p\right)S_0 = \varepsilon\sigma T_a^4 + (1-\varepsilon)\sigma T_s^4 = \sigma T_e^4 \qquad (2.10)$$

Eqs. (2.9) and (2.10) lead to:

$$\sigma T_s^4 = \frac{2}{2-\varepsilon}\frac{1}{4}\left(1-\alpha_p\right)S_0 = \frac{2}{2-\varepsilon}\sigma T_e^4 \qquad (2.11)$$

$$T_s = \left(\frac{2}{2-\varepsilon}\right)^{\!\frac{1}{4}} T_e \qquad (2.12)$$

For $\varepsilon=0$, corresponding to an atmosphere totally transparent to infra-red radiations $T_s=T_e$, which is well in agreement with the result of section 2.1. For a perfect **black body**, we get a result identical to Eq. (2.7), as expected. A typical value of 0.97 for the atmosphere provides a value of $T_s=1.18\ T_e$, i.e. 301 K (28°C). We can also compute T_a as:

$$T_a = \left(\frac{1}{2-\varepsilon}\right)^{\!\frac{1}{4}} T_e = \left(\frac{1}{2}\right)^{\!\frac{1}{4}} T_s \qquad (2.13)$$
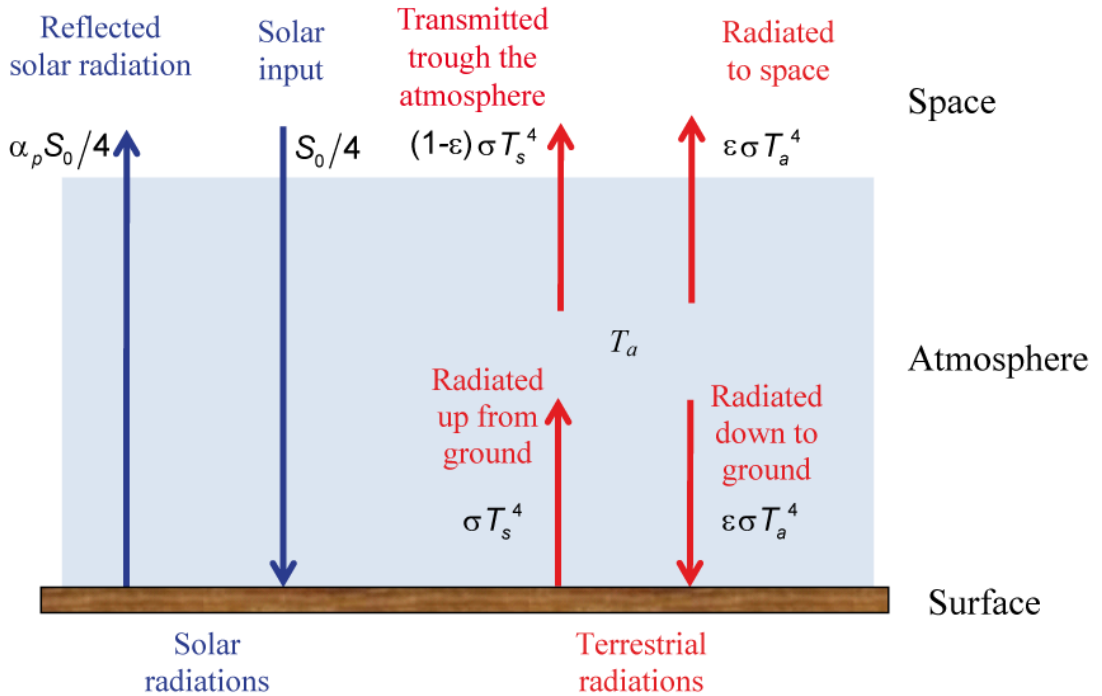

Figure 2.5: Heat balance of the Earth with an atmosphere represented by a single layer totally transparent to solar radiation and with an infrared emissivity ε.

2.1.3 Present-day insolation at the top of the atmosphere

The instantaneous **insolation**, defined as the energy received per unit time and unit surface on a horizontal plane at the top of the atmosphere (or on a horizontal plane at the Earth's surface, if we neglect the influence of the atmosphere) depends on the geographical position on Earth as well as on the position of the Earth relative to the Sun. The influence of those factors is described in the following sections.

2.1.3.1 Earth's orbit around the Sun.

According to Kepler's first law, the Earth's trajectory around the Sun is an ellipse with the Sun at one focus.
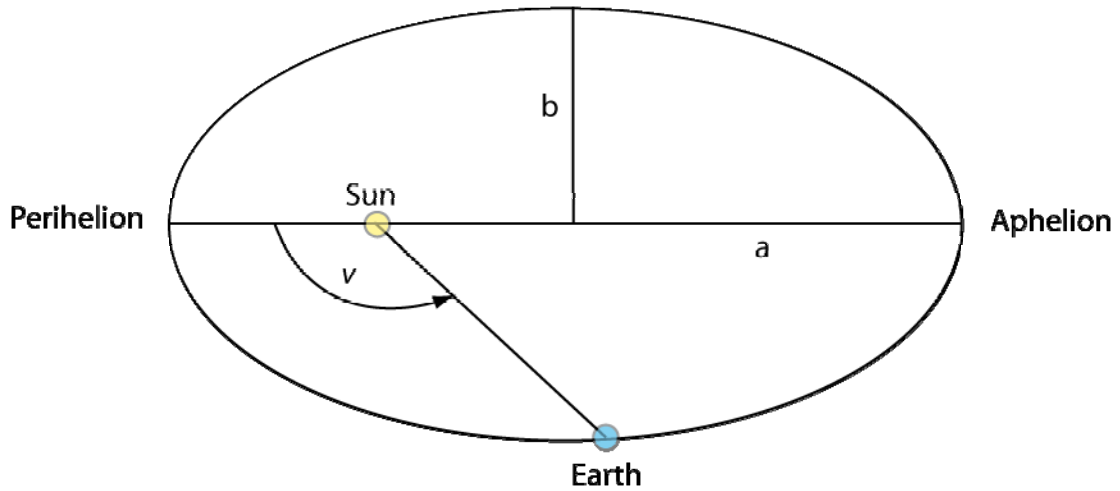

Figure 2.6: Schematic representation of the Earth's orbit around the Sun. The eccentricity has been exaggerated for clarity.

The point of the Earth's orbit that is the closest to the Sun is called the **perihelion** while the **aphelion** is the point that is farthest from the Sun (Fig. 2.6). a is half of the major axis and b half of the minor axis. The shape of the ellipse is then characterised by its **eccentricity** (ecc), defined by:

$$ecc = \frac{\sqrt{(a^2 - b^2)}}{a} \qquad (2.14)$$

The parameters of the Earth's orbit vary with time (see section 5.4.1) but at present ecc=0.0167, meaning that the Earth's orbit is very close to a circle (which of course corresponds to an eccentricity of zero).

The distance from the Sun to the Earth (r) can be computed as a function of v, the true anomaly, according to the formula for an ellipse:

$$r = \frac{a(1 - ecc^2)}{1 + ecc \cos v} \qquad (2.15)$$

The amount of incoming solar electromagnetic radiation per unit area at the top of the atmosphere is a function of r. We can define r_m as the mean distance between the Earth and the Sun by:

$$r_m = \sqrt{ab} = a\ \sqrt{(1 - ecc^2)} \tag{2.16}$$

This means that a circle with radius r_m would have the same area as the ellipse corresponding to the Earth's orbit. The total energy emitted by the Sun is equal to the total energy received on the surface of a sphere of radius r, centred on the Sun, and to that received on a sphere of radius r_m. S_r the amount of solar radiation per unit area measured on the outer surface of the Earth's atmosphere in a plane perpendicular to the rays at a distance r from the Sun can then be computed as a function of the Solar Constant S_o:

Total energy emitted by the Sun measured at a distance $r_m=$
Total energy emitted by the Sun measured at a distance r

$$4\pi r_m^2 S_0 = 4\pi r^2 S_r \tag{2.17}$$

$$S_r = \frac{r_m^2}{r^2} S_0 \tag{2.18}$$

2.1.3.2 Computation of the zenith angle.

As the rotation axis of the Earth is not perpendicular to its orbital plane, the **ecliptic plane**, which is the geometric plane containing the mean orbit of the Earth around the Sun, is inclined relative to the **celestial equatorial plane**, which is the projection of the Earth's equator into space. This angle is called the **obliquity** of the ecliptic ε_{obl}. At present, it is about 23°26' (Fig. 2.7).
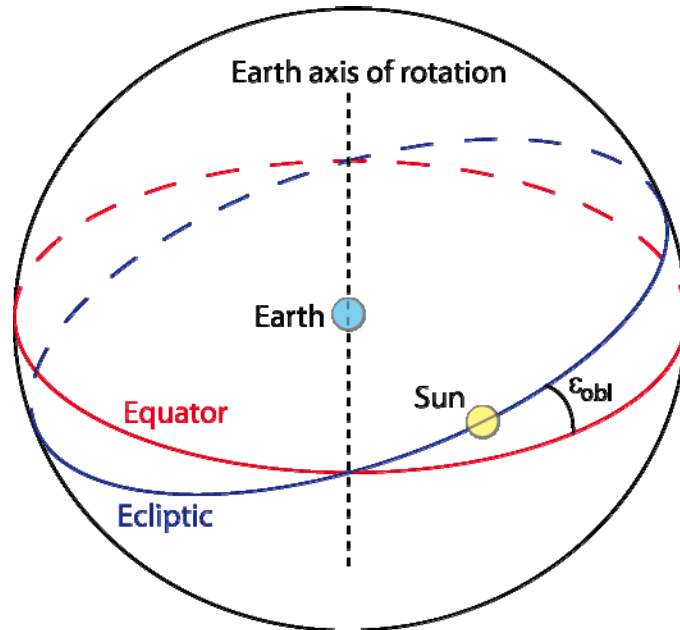

Figure 2.7: Representation of the ecliptic and the obliquity ε_{obl} in a geocentric system.

The intersections of those two planes are used to define the seasons. In particular, the **vernal equinox**, which is often used as a reference in the coordinate system to define the **true longitude** λ_t (or ecliptic longitude, Fig. 2.8.), corresponds to the intersection of the ecliptic plane with the celestial equator when the Sun moves from the austral to the boreal hemisphere in its apparent movement around the Earth. This occurs around March 20-21 and is often called the spring equinox. However, this term could be misleading as this date corresponds to the beginning of autumn in the Southern Hemisphere.

By definition the **vernal equinox** corresponds to a true longitude equal to zero, the solstices to the true longitudes equal to 90° and 270° and the 'autumn' equinox to a true longitude equal to 180°. If we define *PERH* as the longitude of the perihelion measured from the autumn equinox (*PERH*= 102.04 in present-day conditions, corresponding to a true longitude of 180°+PERH=282.04), we can write

$$\lambda_t = 180 + PERH + v \tag{2.19}$$

This definition can be used to compute the length of the different seasons, using Kepler's second law which states that, as the Earth moves in its orbit, a line from the Sun to the planet sweeps out equal areas in equal times.
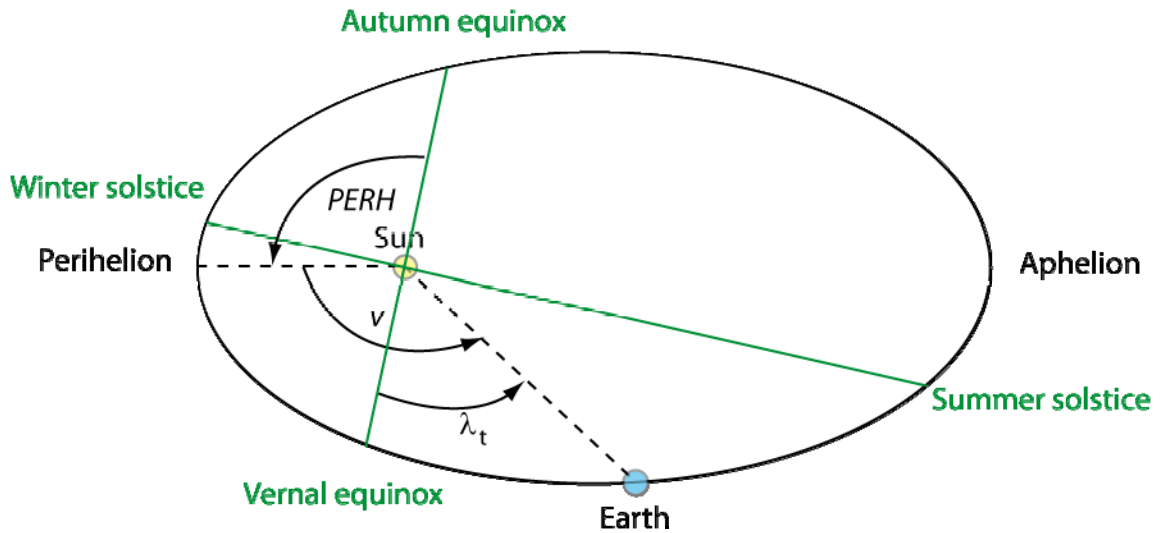

Figure 2.8: Representation of the true longitudes and the seasons in the ecliptic plane.

S_h, the amount of solar energy received per unit time on a unit horizontal surface at the top of the atmosphere is proportional to the cosine of θ_s, the solar **zenith distance** which is defined as the angle between the solar rays and the normal to the Earth's surface at any particular point.

$$S_h = S_r \cos \theta_s \tag{2.20}$$

S_h rises as $\cos \theta_s$ becomes closer to 1, i.e. as the horizontal surface becomes more normal to the Sun's rays. When the surface is inclined at an oblique angle to the solar rays, the amount of energy received by the surface per square metre is lower, because the total amount of energy received by the perpendicular surface ($S_r A_1$ on Fig. 2.9) is distributed across a larger surface ($S_r A_1 = S_h A_2 = S_h A_1 / \cos \theta_s$).
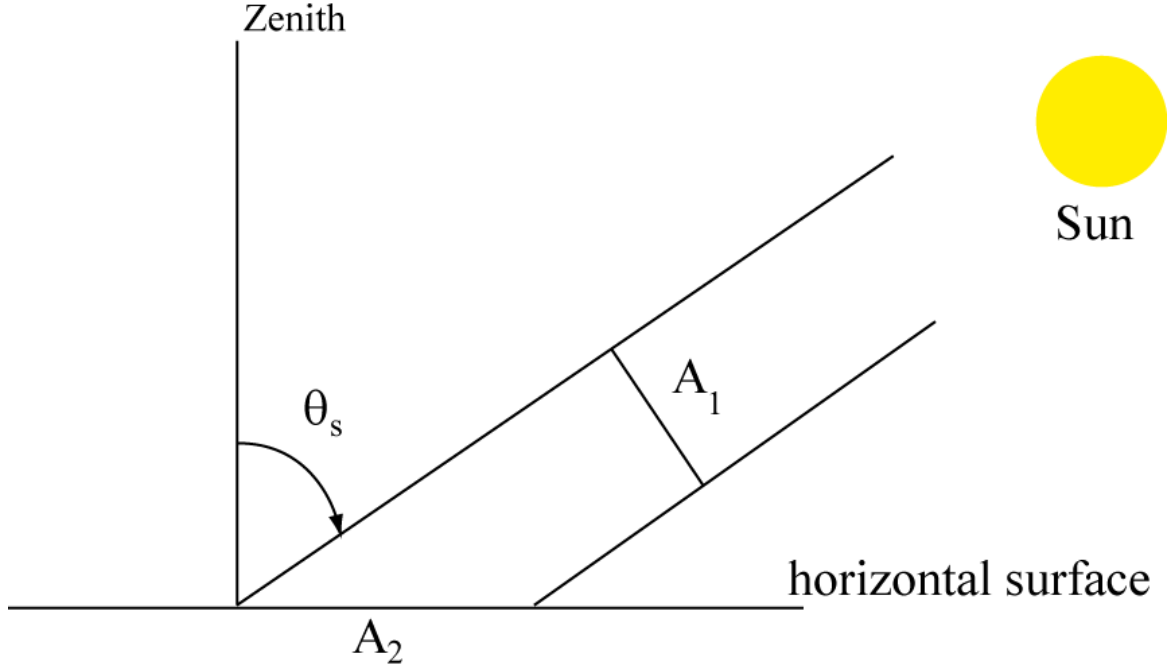
Figure 2.9: Influence of the zenith angle on the amount of radiation received on a horizontal surface. A_1 is the surface perpendicular to the solar beam while A_2 is the horizontal surface illuminated by the rays crossing A_1.

$\cos\theta_s$ can be computed using standard astronomical formula:

$$\cos\theta_s = \sin\phi\sin\delta + \cos\phi\cos\delta\cos HA \qquad (2.21)$$

where ϕ is the latitude of the point on Earth, δ is the solar declination, HA is the hour angle. The declination δ is defined as the angle between a line from the centre of the Earth towards the Sun and the celestial equator (Fig. 2.10). It varies from $+\varepsilon_{obl}$ at the summer solstice in the Northern Hemisphere to $-\varepsilon_{obl}$ at the winter solstice and zero at the equinoxes. During the day, its value is constant to a very good approximation. Knowing the true longitude and the obliquity, the declination δ can be estimated using the formula:

$$\sin\delta = \sin\lambda_t \sin\varepsilon_{obl} \qquad (2.22)$$

Furthermore, if we denote the number of the day, starting on the first of January, by NDAY, the value of δ can also be estimated by using the raw approximation (zero order to eccentricity):

$$\delta = 23.45°\sin\left(360°\left(NDAY - 80\right)/365\right) \qquad (2.23)$$

The hour angle HA indicates the time since the Sun was at local meridian, measured from the observer's meridian westward. HA is thus zero at the local solar noon. It is generally measured in radians or in hours (2π rad=24 hours). It could more formally be defined as the angle between the half plane determined by the Earth's axis and the zenith (local meridian half-plane), and the half plane determined by the Earth's axis and the Sun.
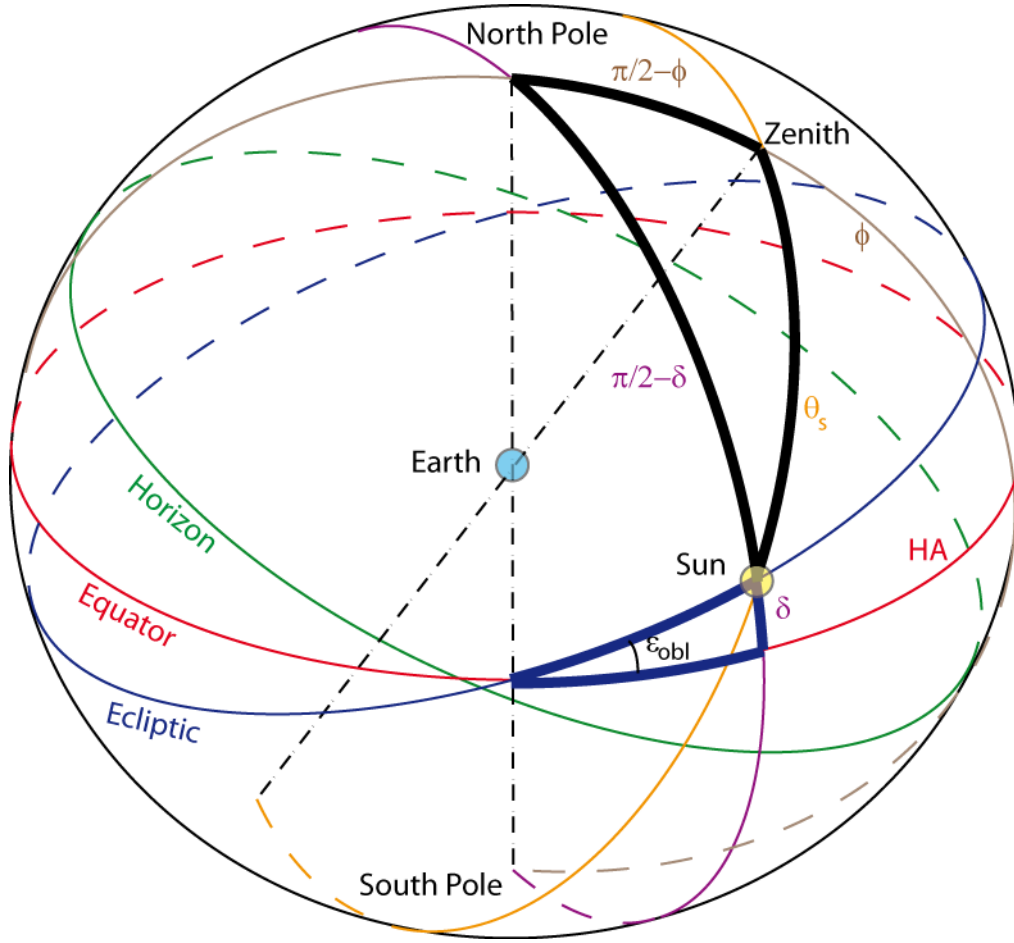
Figure 2.10: Representation of the declination and of the hour angle in a geocentric system. On this figure, the equator and the ecliptic are fixed. The apparent motion of the Sun corresponds to a complete revolution along the ecliptic in one year. The hour angle (and the location of the local meridian (brown circle) through the North Pole and the zenith) change as the Earth makes a complete rotation around its axis in 1 day. Applying the standard spherical trigonometric rules to the black bold triangle allows Eq. 2.21 to be demonstrated. This figure can also be used to demonstrate Eq. 2.22, using the blue bold triangle.

2.1.3.3 Daily insolation at the top of the atmosphere.

If the Sun rises above the horizon on a particular day, we can compute the times of sunrise (HA_{sr}) and sunset (HA_{ss}) using Equation 2.21, since both events correspond to a solar zenith angle of 90°:

$$HA_{SR,SS} = \pm \arccos\left(-\tan\phi\tan\delta\right) \qquad (2.24)$$

The length of the day (*LOD*) is then given by

$$LOD = \frac{24}{\pi}\arccos\left(-\tan\phi\tan\delta\right) \qquad (2.25)$$

The coefficient $24/\pi$ is used to convert the result from radians for *HA* to hours for *LOD*.

At the equator, since ϕ is equal to zero, *LOD* is always equal to 12 hours. At the equinoxes, δ is equal to zero so *LOD* is equal to 12 hours everywhere. We can also estimate from Eq. 2.25 that in the polar regions of the Northern Hemisphere, where $\phi + \delta \geq 90°, \tan\phi\tan\delta \geq 1$ in summer, the Sun is visible during the whole day (midnight sun) where $\phi - \delta \geq 90°, \tan\phi\tan\delta \leq -1$ in winter, the Sun is always below the horizon (polar night). Similar formulae can be obtained for the Southern Hemisphere.
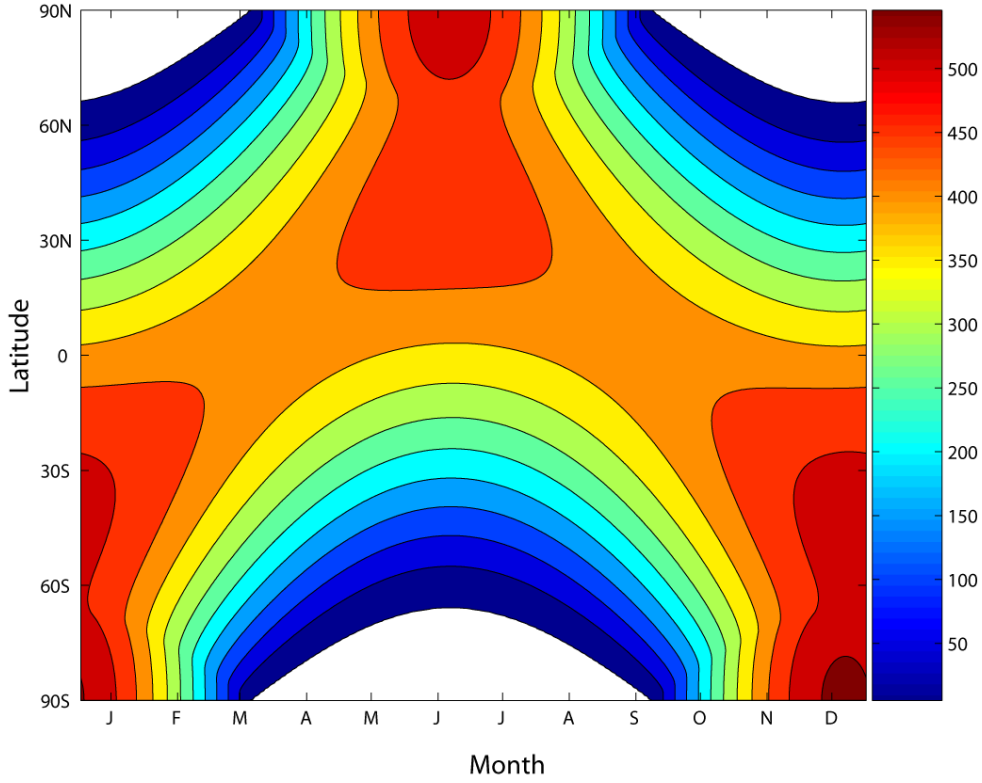

Figure 2.11: Mean daily insolation (in W/m^2) on a horizontal surface at the top of the atmosphere as a function of the day of the year and the latitude. White areas correspond to the polar night.

Using Eqs 2.18, 2.20, 2.21, and 2.24, we can integrate S_h over time to compute $S_{h,day}$ the daily insolation on a horizontal surface (in J m^{-2}). The mean insolation over one day (in W/m^2) is also often used. It is simply $S_{h,day}$ divided by 24 hours

$$
\begin{aligned}
S_{h,day} &= S_0 \frac{r_m^2}{r^2} \int_{Sunrise}^{Sunset} \left(\sin\phi\sin\delta + \cos\phi\cos\delta\cos HA\right) dt \\
&= S_0 \frac{r_m^2}{r^2} \frac{86400}{2\pi} \int_{HA_{SR}}^{HA_{SS}} \left(\sin\phi\sin\delta + \cos\phi\cos\delta\cos HA\right) dHA \qquad (2.26) \\
&= S_0 \frac{r_m^2}{r^2} \frac{86400}{\pi} \left(HA_{SS}\sin\phi\sin\delta + \cos\phi\cos\delta\sin HA_{SS}\right)
\end{aligned}
$$

As expected, the daily insolation is higher in the summer hemisphere because of the lower zenith distance (i.e. a Sun higher above the horizon) and longer duration of the day. Averaged over one day, the maximum solar insolation occurs at the poles at the summer

solstice (see Fig. 2.11), while averaged over one year the solar energy received at the top of the atmosphere at the equator is about twice that received at the poles.

2.1.4 The heat balance at the top of the atmosphere: geographical distribution

The geographical distribution of the net incoming solar radiation at the top of the atmosphere (i.e., the incoming minus the reflected solar radiation) that is absorbed by the Earth is a function of the insolation distribution as well as of the regional variations of the planetary **albedo** (Fig. 2.12). The latter is influenced by several factors, including the **albedo** of the surface (see section 1.5) and the presence of clouds which reflect a significant fraction of the incoming solar radiation back to space. The influence of clouds is particularly evident in the Tropical Regions, where it explains, for instance, why the absorbed solar radiation is larger in the relatively cloud free eastern Equatorial Pacific than in the cloudier western Pacific. At high latitudes, the surface albedo is high because of the high zenith distance (Sun low above the horizon) and the high reflectance of snow and ice (see section 1.4). This high surface albedo at high latitudes amplifies the latitudinal variations in solar radiation associated with the Earth's geometry (Fig. 2.11), resulting in a difference of nearly a factor of five in annual mean absorbed solar radiation at the poles, compared to the equator.
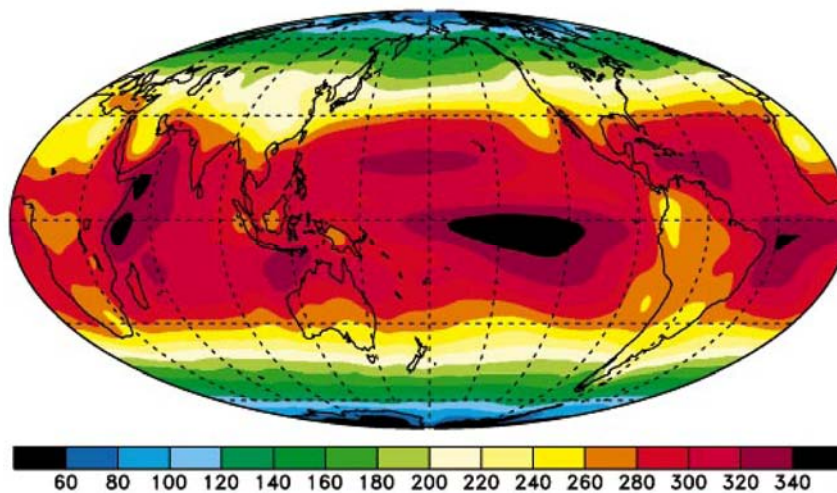

Figure 2.12: Annual mean net incoming solar radiation at the top of the atmosphere that is absorbed by the Earth (in W/m^2). Figure from Trenberth and Stepaniak (2003). Copyright 2003 American Meteorological Society (AMS).

The **Stefan-Boltzmann law** says that the **longwave radiation** emitted is a function of the temperature of the emitting surface. A difference of about 50°C between the equator and the poles roughly corresponds to a variation in the emitted thermal radiation of about 50 W/m^2, which is in reasonable agreement with the estimated values (Fig. 2.13). The presence of clouds and water vapour also has a large influence. Indeed, water vapour is a strong greenhouse gas. It absorbs part of the infra-red radiation emitted by the surface before re-emitting radiation, generally at a lower temperature as clouds are located higher in the atmosphere (see section 2.1.2). This results in less outgoing longwave radiation. As a consequence, the maximum outgoing longwave radiation is found above warm dry areas such as the subtropical deserts. More generally, wet equatorial areas generally emit less radiation than dry tropical areas (Fig. 2.13).
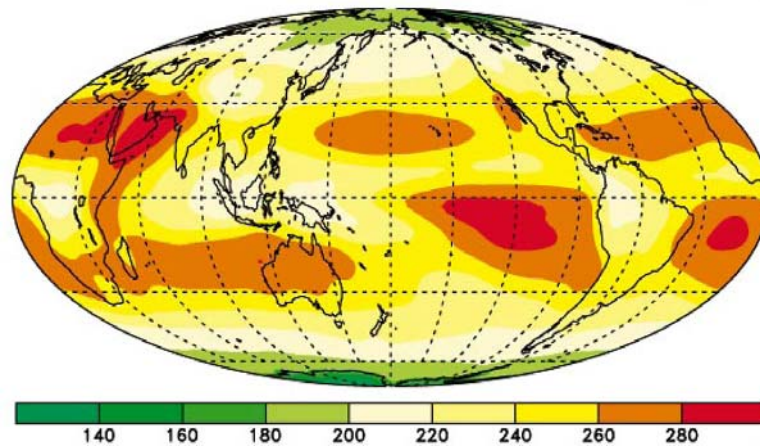
36

Figure 2.13: Net annual mean outgoing longwave radiation at the top of the atmosphere (in W/m^2). Figure from Trenberth and Stepaniak (2003). Copyright 2003 American Meteorological Society (AMS).
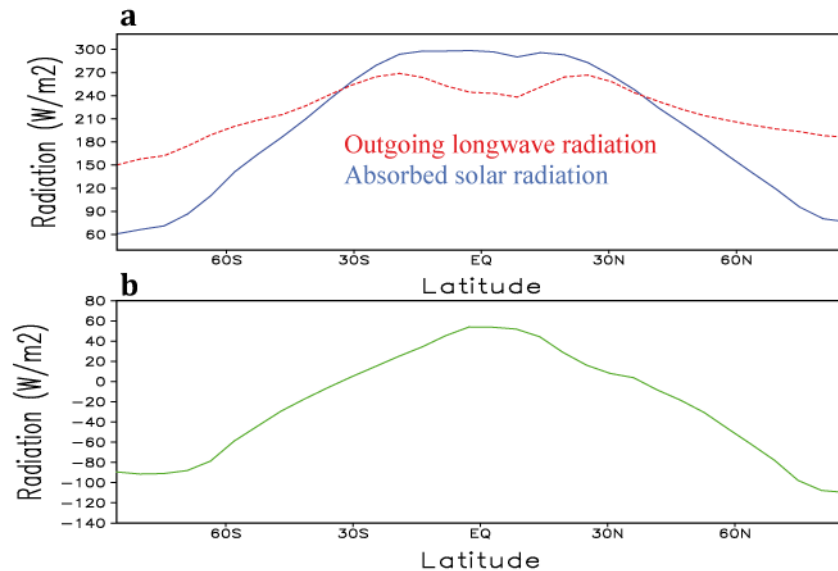

Figure 2.14: (a) **Zonal mean** of the absorbed solar radiation (blue) and the outgoing longwave radiation (dashed red) at the top of the atmosphere in annual mean (in W/m^2). (b) **Zonal mean** of the difference between the absorbed solar radiation and the outgoing longwave radiation at the top of the atmosphere in annual mean (in W/m^2). Data from NCEP-NCAR **reanalysis** (Kalnay et al. 1996).

When averaged over longitude, the outgoing **longwave radiation** clearly shows less latitudinal variation than the net incoming solar radiation absorbed by the Earth. As a consequence, the absorbed solar radiation outbalances the outgoing radiation in regions located between roughly 40°S and 40°N, while a net deficit in the net radiative flux at the top of the atmosphere (RF_{TOA}) is observed poleward of 40°N and 40°S (Fig. 2. 14). RF_{TOA} also displays some longitudinal variations, the most spectacular being probably the net negative flux over the Sahara because of the dry conditions there and of the high albedo of its sand.
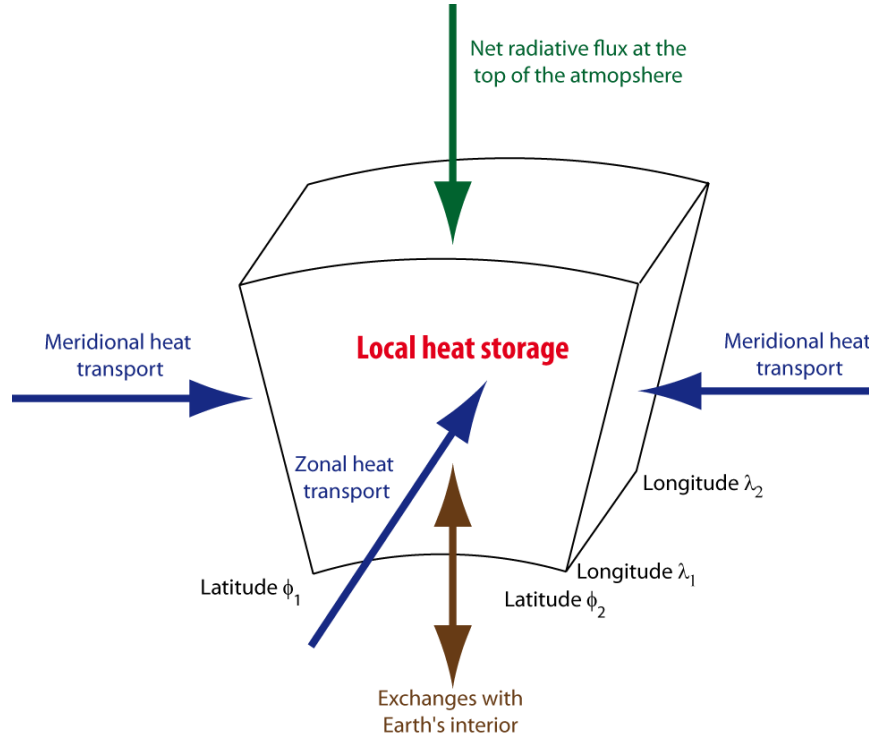
37

Figure 2.15: Schematic representation of the heat balance for the atmosphere, ocean, land surface and the ground in a volume lying between latitudes ϕ_1, ϕ_2 and longitudes λ_1, λ_2.

2.1.5 Heat storage and transport

In an area delimited by latitudes ϕ_1, ϕ_2 and longitudes λ_1, λ_2 (Fig. 2.15), the net radiative heat flux at the top of the atmosphere RF_{TOA} must be balanced by the sum of the horizontal heat transport, the heat exchanges with the deep ground, and the contribution to the heat budget associated with changes in the heat storage in the atmosphere, the ocean and the ground. As the ground has a very low thermal conductivity, only the top few metres interact with the surface on seasonal to decadal **timescales**. In the majority of climatic applications, it is thus sufficient to take the top few metres of the ground (typically 10 metres) into account, and assume that exchanges with the deep ground or the Earth's interior can be represented by a geothermal heat flux. The value of this flux is weak in the majority of the regions (~0.075 W/m^2) and it is thus often neglected in heat balance computations.

2.1.5.1 Heat storage.

On daily and seasonal timescales, the heat storage by the climate system plays a large role in mitigating the influence of the changes in the radiative flux at the top of the atmosphere. Those variations in heat storage for the ocean, atmosphere and ground can be estimated by:

$$\text{rate of change in heat storage} = \int_V \rho c_m \frac{\partial T}{\partial t} dV \qquad (2.27)$$

where ρ, c_m and T are the density, specific heat capacity and temperature of the media (i.e. atmosphere, sea or ground) included in the volume V. This term can be approximated by:

$$\text{rate of change in heat storage} \simeq m_m c_m \frac{\partial T_m}{\partial t} = C_m \frac{\partial T_m}{\partial t} \qquad (2.28)$$

where m_m, c_m and T_m are the characteristic mass, specific heat capacity and temperature of the media that is storing heat and C_m is the effective heat capacity of the media (measured in J m^{-2} K^{-1}). The value of m_m is strongly dependent on the volume that displays significant changes in heat content on the **timescale** of interest.

On the seasonal **timescale**, the heat content of the whole atmosphere changes. If we use a value for c_p of 1000 J K^{-1} Kg^{-1} and a mass of 10^4 kg m^{-2} (assuming **hydrostatic equilibrium**, this corresponds roughly to a pressure of 10^5 Pa), we get an estimate of C_m for the atmosphere of:

$$C_{m,atmosphere} = 1000 \cdot 10^4 = 10^7 \text{ J K}^{-1}\text{m}^{-2} \qquad (2.29)$$

Only the top 50 to 100 metres of the sea display a significant seasonal cycle in temperature. Using a specific heat capacity of water of 4000 J K^{-1} kg^{-1}, and a mass of 7.5 10^4 kg m^{-2},(i.e. 75 m times 1000 kg m^{-3}), we have.

$$C_{m,ocean} = 4000 \cdot 7.5\ 10^4 = 3.\ 10^8 \text{ J K}^{-1}\text{m}^{-2} \qquad (2.30)$$

The ground has a specific heat capacity similar to that of the ocean but only a few metres are affected by the seasonal cycle. As a consequence, the effective heat capacity of the ground is much lower than that of the ocean on this time scale.

This rough comparison clearly shows that the effective thermal capacity of the sea is an order of magnitude larger than that of the atmosphere and the ground on a seasonal timescale. As a consequence, the sea stores much more energy during summer than the other media, energy that is released during winter. This moderates the amplitude of the seasonal cycle over the sea, by comparison with the land. A strong difference in the amplitude of the seasonal cycle is also seen in land areas that are directly influenced by the sea (at mid-latitudes, because of the westerly winds, this means land masses to the east of the oceans, such as Europe) compared to land masses far away from sea (Fig. 2.16). A similar analysis on a daily timescale shows that, heat storage by land, sea and atmosphere are all important.
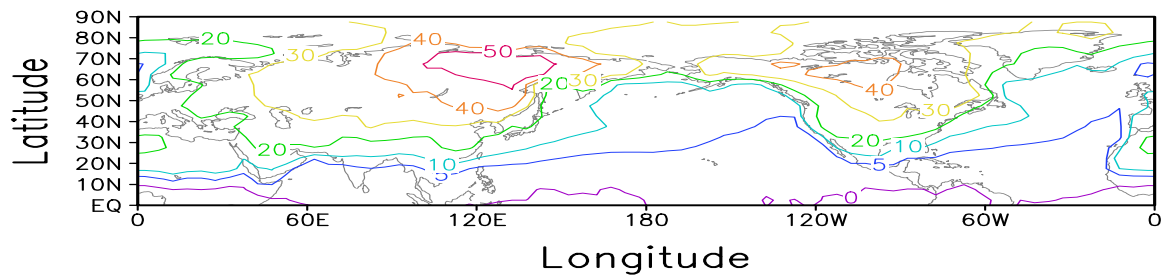

Figure 2.16: Amplitude of the seasonal cycle in surface temperature (in °C) in the northern hemisphere measured as the difference between July and January monthly mean temperatures. Data from the HadCRUT2 dataset (Rayner et al., 2003).

For decadal to centennial variations, such as the warming observed since the mid 19th century, thermal heat storage in the first hundred metres depth of the ocean (and at greater depths in regions of **deep water formation**) also moderates the transient temperature changes (see Chapter 6). On much longer time scales, such as the glacial-interglacial cycles, we have to take into account the full depth of the ocean (~4000 m). For deglaciation, which is faster than the glacial inception (see Chapter 5), we can estimate the order of magnitude of the mean ocean temperature at a 2°C change in 5000 years. This corresponds to a mean heat flux at the ocean surface of 0.03 W m^{-2} (= 4000 m . 1000 kg m^{-3} . 4000 J K^{-1} kg^{-1} . 3°C / [5000 . 365 . 24 . 3600 s]). This demonstrates that the change in oceanic heat storage plays a negligible role but the inertia of the ice sheets has to be taken into account on these timescales.

2.1.5.2 Heat transport.

Locally, heat storage by the **climate system** cannot compensate for the net radiative flux imbalance at the top of the atmosphere and, annually, the balance is nearly entirely achieved by heat transport from regions with a positive net radiative flux to regions with a negative net radiative flux. When the balance is averaged over latitudinal circles (**zonal mean**), this corresponds to a **meridional** heat transport from equatorial to polar regions (Fig. 2.17). This poleward heat transport at a latitude ϕ can be estimated by integrating the net radiative balance at the top of the atmosphere from the South Pole to latitude ϕ :

$$RT(\phi) = \int_{-\pi/2}^{\phi} \int_{0}^{2\pi} RF_{TOA}\left(\lambda, \phi'\right) R^2 \cos\phi' d\lambda d\phi' \qquad (2.31)$$
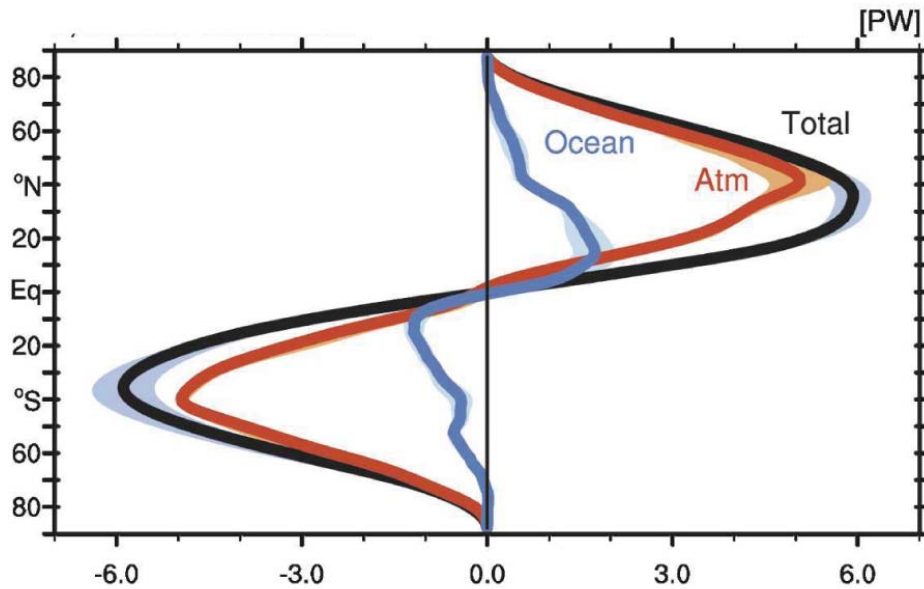
Figure 2.17: The required total (RT) heat transport in PW (10^{15} W), needed to balance the net radiation imbalance at the top of the atmosphere (in black) and the repartition of this transport in oceanic (blue) and atmospheric (red) contributions, accompanied with the associated uncertainty range (shaded). A positive value of the transport on the x axis corresponds to a northward transport. Figure from Fasullo and Trenberth (2008). Copyright 2008 American Meteorological Society (AMS).

The heat transport obtained is nearly zero at the equator, rising to more than 5 PW at latitudes of about 35°, before declining again towards zero at the poles (Fig. 2.17). It can be divided into an oceanic and an atmospheric contribution, the horizontal transport on continental surface being negligible. This shows that, except in tropical areas, the atmospheric transport is much larger than the oceanic transport.

The energy can be transported as **sensible heat** (c_pT, which is related to **internal energy**), potential energy (gz), **latent heat** (Lq) and kinetic energy ($0.5\ u^2$) and is expressed per unit of mass as:

$$E = c_pT + gz + L_vq + 0.5u^2 \tag{2.32}$$

where z is the altitude (or depth), L_v the latent heat of vaporisation of water, q the **specific humidity** and u the velocity of the media. The first term is often called **sensible heat**. The transport of kinetic energy is much weaker than the other transports and is generally neglected. In the atmosphere, the three remaining terms must be taken into account, but in the ocean the transport of sensible heat is clearly dominant. Moreover, in some special cases, an additional term representing the transport of latent heat by sea ice and icebergs must be considered for local or regional analyses at high latitudes.

In the tropics, the majority of the atmospheric poleward heat transport is achieved by the **Hadley circulation**. By contrast, the mean circulation plays a much weaker role at mid to high latitudes where nearly all the transport is effected by **eddies**. In the ocean, both the wind-driven and deep-oceanic circulation are responsible for a significant part of the oceanic poleward heat transport, the latter having a dominant influence in the tropics. The role of the oceanic **eddies** is less well known, but they can be significant in at least some regions (such as the Southern Ocean).

In addition to its dominant role in the reduction of the temperature contrast between the equator and the poles on Earth (compared to a planet without an ocean and an atmosphere), horizontal heat transport is also responsible for some temperature differences on a regional scale. This can be illustrated by analysing the departure of the local temperature from to the **zonal** mean temperature. At first sight, Fig 2.18 emphasises the mountainous area such as the Tibetan Plateau, the Rocky Mountains and Greenland, where the temperature is much lower than at other locations at the same latitude. However, the influence of the atmospheric circulation is also clearly apparent with, for instance, in cold areas such as north-east Canada. This is because the dominant winds have a strong northerly component in this region, while the North Atlantic is warmer, partly because of the south-westerly winds in this region (see section 1.2). Over the ocean, the influence of the northward western boundary currents (see section 1.3) results in generally warmer surface oceanic temperature at about 30-40°N in the western part of the basin than in the eastern part (where the oceanic currents are generally bringing colder water from the North).

The **thermohaline circulation** is an additional source of longitudinal asymmetry as, in the Northern Hemisphere, **deep water formation** only occurs in the North Atlantic and not in the North Pacific (see section 1.3). The associated circulation transports cold water southward at great depths with the mass balance ensured by a corresponding northward transport of warmer water in the surface layer. This results in a net oceanic transport in the North Atlantic of about 0.8 PW at 30°N (i.e. more than twice the estimated transport in the wider Pacific at the same latitude). The **thermohaline circulation** is also responsible for the northward oceanic heat transport at all latitudes in the Atlantic, even in the Southern Hemisphere.
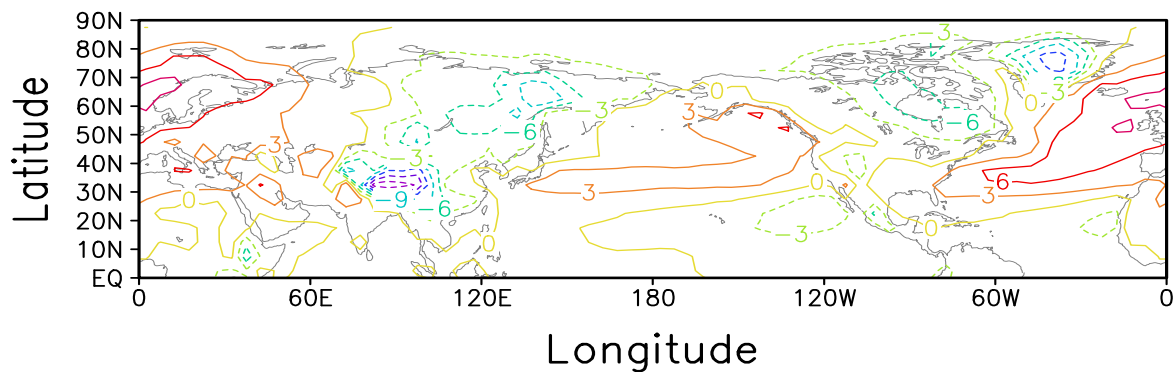
Figure 2.18: Difference between the annual mean surface temperature and the **zonal mean** temperature(computed as the annual mean temperature measured at one particular point minus the mean temperature obtained at the same latitude but averaged over all possible longitudes). Data from the HadCRUT2 dataset (Rayner et al., 2003).

This oceanic heat transport contributes to the fact that higher temperatures are observed in the North Atlantic than in other oceanic basins. Its influence is particularly large in the Barents Sea, north of Norway. Thanks to the oceanic heat transport, this area located north of 70°N (i.e., at the same latitude as the northern part of Alaska) remains free of sea ice all year long. Climate model calculations have shown that, if deep water formation was suppressed in the North Atlantic, the temperature in the North Atlantic and in Western Europe would be reduced by about 3° C at 45° N, while the annual mean temperature would decrease by more than 15° C in northern Norway and the Barents Sea.

2.1.6 Heat balance at the surface

As discussed in section 2.1.1, the incoming solar radiation on a horizontal surface at the top of the atmosphere is about 342 W m^{-2}, with roughly 30% of this being reflected back into space. An analysis of the Earth's global heat balance (Fig. 2.19) shows that more that 70% of the reflection takes place in the atmosphere, mainly because of the presence of clouds and **aerosols**. The remaining 30% is reflected by the surface. By contrast, the majority of the absorption of solar radiation occurs at the surface, which absorbs 2.5 times more solar energy than the whole atmosphere. This shows clearly that the majority of atmospheric warming occurs from below, and not by direct absorption of solar radiation. This important property of the system explains the major characteristics of the Earth's atmosphere, including the vertical temperature profile and the large scale circulation of the atmosphere (see section 1.2).

The outgoing **longwave radiation** required to balance the Earth's budget at the top of the atmosphere is mainly emitted by the atmosphere and clouds. Among the 396 W m^{-2} emitted by the surface, only 40 W m^{-2} can exit the **climate system** directly. The large majority of surface longwave radiation is absorbed by the atmospheric greenhouse gases and re-emitted towards the surface where the downward longwave radiation flux (333 W m^{-2}) becomes the largest term in the surface heat balance.

In addition to the radiative fluxes, the surface and the atmosphere exchange heat through direct contact between the surface and the air (**sensible heat** flux or thermals) as well as through evaporation and transpiration. Indeed, when evaporation (or sublimation) takes place at the surface, the **latent heat** required for the phase transition is taken out of the surface and results in a surface cooling. Later, mainly during the formation of clouds,

the water vapour condensates and the latent heat is released into the atmosphere. This leads to a net mass and heat transfer from the surface into the atmosphere, which is one of the main drivers of the general atmospheric circulation.
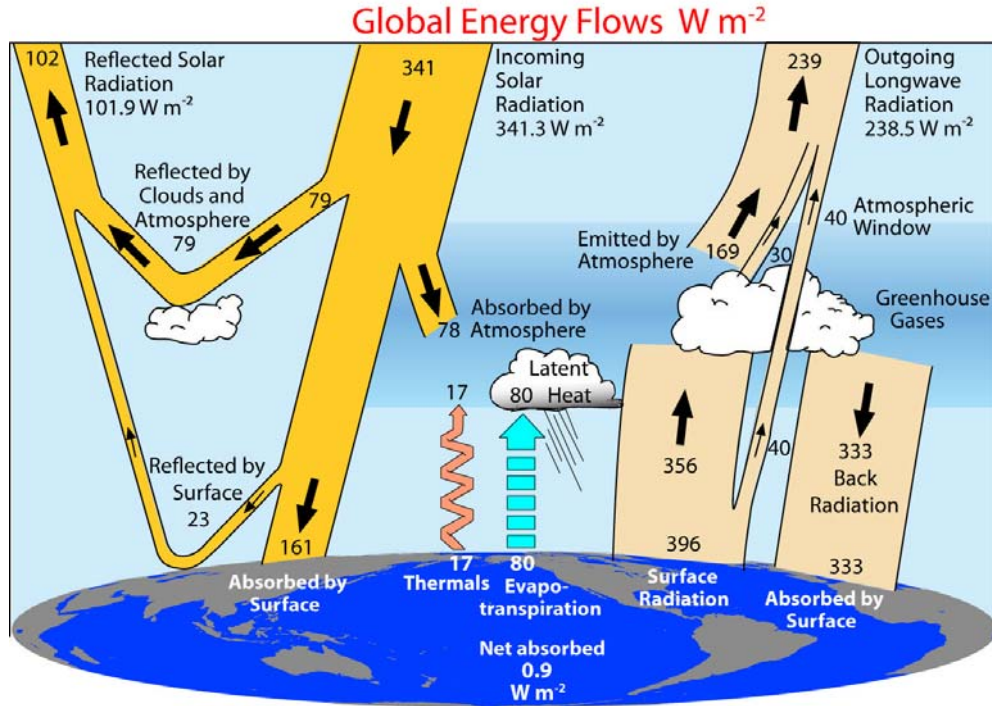

Figure 2.19: Estimate of the Earth's annual and global mean energy balance for the March 2000 to May 2004 period in W m^{-2}. Figure from Trenberth et al. (2009). Copyright 2009 American Meteorological Society (AMS).

The fluxes of sensible and latent heat are generally estimated as a function of the wind speed at a reference level, and the difference in temperature (for the sensible heat flux F_{SH}) or specific humidity (for the latent heat flux F_{LH}) between the surface and the air at this reference level, using classical bulk aerodynamic formulae:

$$F_{SH} = \rho c_p c_h U_a \left(T_s - T_a \right) \tag{2.33}$$

$$F_{LE} = \rho L_v c_L U_a \left(q_s - q_a \right) \tag{2.34}$$

where U_a, T_a, q_a are the wind velocity, air temperature and specific humidity at the reference level (generally 2 m or 10 m), T_s and q_s are the surface temperature and **specific humidity** at the surface, and c_h and c_L are the aerodynamic (bulk) coefficient. In general, they are function of the stability of the **atmospheric boundary layer**, the roughness of the surface, the wind speed and the reference height. In the majority of cases, c_h and c_L are not too different from each other and their value ranges from $1 \ 10^{-3}$ to $5 \ 10^{-5}$. The highest values occur with unstable boundary layers and very rough surfaces which tend to generate strong turbulent motions and thus higher exchanges between the surface and the air than quieter situations.

The **specific humidity**, q_s, above a wet surface is generally very close to saturation. It can thus be expressed using the **Clausius-Clapeyron equation**, which shows that the amount of water vapour in the air at saturation is strongly dependent on temperature. For

instance, the amount of water vapour that can be present in the atmosphere at a temperature of 20°C is more than three times higher than at 0°C. As a consequence, the evaporation and the latent heat flux are much larger at low latitudes than at high ones. The latent heat flux is thus larger than the sensible heat flux at low latitudes, while the two fluxes are generally of the same order of magnitude over the ocean at high latitudes. The ratio between the sensible heat and latent heat fluxes is usually expressed as the Bowen Ratio B_o:

$$B_o = \frac{F_{SH}}{F_{LE}} \tag{2.35}$$

Over land surfaces, the latent heat flux is a function of the water availability and B_o can be much higher than unity over dry areas.

The heat balance shown in Figure 2.19 for the whole Earth can also be computed for any particular surface on Earth. This is generally the method used to obtain T_s. Let us consider a unit volume at the Earth's surface with an area of 1 m^2 and a thickness h_{su} (Fig. 2.20). h_{su} is supposed to be sufficiently small to safely make the approximation that the temperature is constant over h_{su} and equal to T_s. The heat balance of this volume can then be expressed as:

$$\rho c_p h_{su} \frac{\partial T_s}{\partial t} = (1 - \alpha) F_{sol} + F_{IR\downarrow} + F_{IR\uparrow} + F_{SE} + F_{LE} + F_{cond} \tag{2.36}$$

The left-hand side of the Eq. 2.36 represents the heat storage in the layer h_{su} (see section 2.1.5). F_{sol} is the incoming solar flux at the surface which is a function of the incoming solar radiation at the top of the atmosphere and of the transmissivity of the atmosphere (related to the presence of clouds, aerosols, the humidity of the air, etc). A fraction α of F_{sol} is reflected by the surface and not absorbed. $F_{IR\downarrow}$ is the downward **longwave** radiation flux at surface. This flux is caused by the emission of infra-red radiation at various levels in the atmosphere. It is thus a complex function of the temperature and humidity profiles in the atmosphere, the cloud cover and the height of the clouds, the presence of various greenhouse gases (in addition to water vapour), etc. The longwave upward radiation flux $F_{IR\uparrow}$ can be computed using the **Stefan-Boltzman law** while the expressions for F_{SE} and F_{LE} are given by Eq. 2.33 and 2.34. F_{cond}, the flux from below the surface, is a conduction flux for solid surfaces (such as the ground and the ice) that can be represented following the **Fourier law**. For the ocean, this flux is related to the dynamics of **the oceanic mixed layer**. Additionally, if the media at the surface is (partly) transparent, a fraction of the radiation is not absorbed in the layer of thickness h_{su} and must be subtracted from the term (1-α F_{sol}) in Eq. 2.36. For the other fluxes, the exchanges take place in a very shallow layer and can reasonably be considered as purely surface processes.

Figure 2.20 displays a relatively simple situation where the surface (i.e. the interface between the atmosphere and the material below) is clearly defined. In complex terrain with very rough topography, for instance over forests or urban areas, defining the lower limit of the atmosphere is less straightforward. Computing the surface fluxes in these regions is a very complex issue which is the currently the subject of intense research.
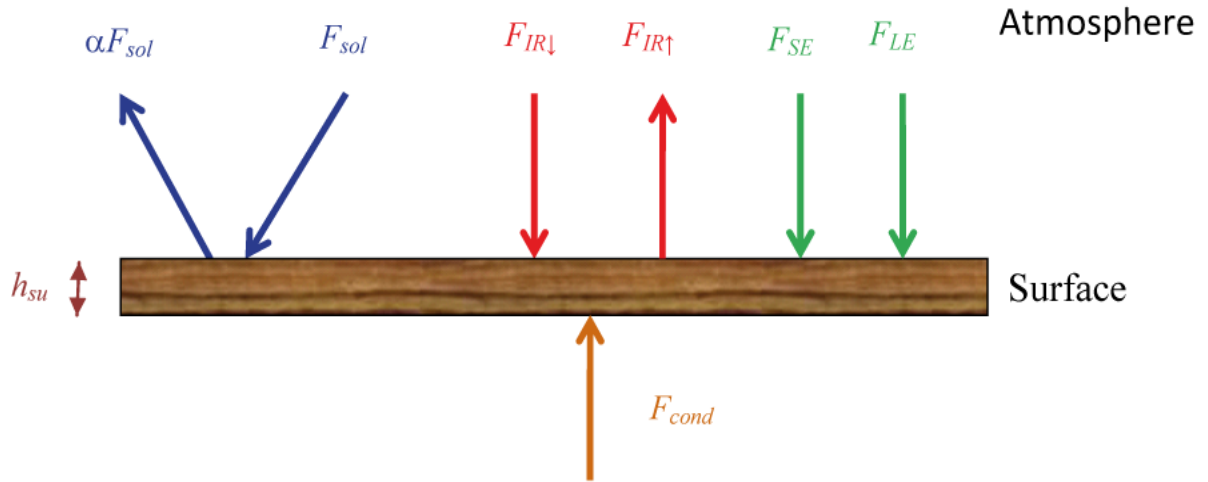
Figure 2.20: The heat balance of a surface.

When snow or ice is present at the surface, the temperature T_s cannot be higher than the freezing point of water. As a consequence, Eq. 2.36 remains valid as long as T_s is below the freezing point. When surface melting occurs (i.e., when T_s equals the freezing point of water) an additional term, corresponding to the latent heat of fusion required to keep the temperature unchanged, must be added to the right-hand side of Eq.2.36.

2.2 The hydrological cycle

As discussed in section 2.1, the water –or hydrological- cycle plays an important role in the energy cycle on Earth. It has a considerable impact on the radiative balance: water vapour is the most important greenhouse gas in the atmosphere (see section 2.1.2); the presence of snow and ice strongly modifies the **albedo** of the surface (see Table 1.3. and sections 2.1.4 and 4.2.3); and clouds influence both the **longwave** and **shortwave** fluxes (see sections 2.1.4, 2.1.6 and 4.2.2). Moreover, water is an essential vehicle for energy: the **latent heat** released during the condensation of water is a dominant heating source for the atmosphere (see section 2.1.6); the transport of water vapour in the atmosphere and of water at different temperatures in the ocean are essential terms in the horizontal heat transport (see section 2.1.5.2).

The hydrological cycle is also essential in shaping the Earth's environment, the availability of water being a critical factor for life as well as for many chemical reactions and transformations affecting the physical environment. Describing the various components of the hydrological cycle and analysing the mechanisms responsible for the exchanges of water between the different reservoirs are thus important elements of climatology.

By far, the largest reservoir of water on Earth is located in the crust, with estimates of the order of 10^{22} kg of water (equivalent to 10^{19} m³ at surface pressure, i.e. about 10 times the amount of water in the oceans, the second largest reservoir). However, exchanges between deep Earth and other reservoirs are so slow that they only have a very weak impact on the hydrological cycle at the surface and are thus generally not taken into account in estimates of the global hydrological cycle (Fig. 2.21).
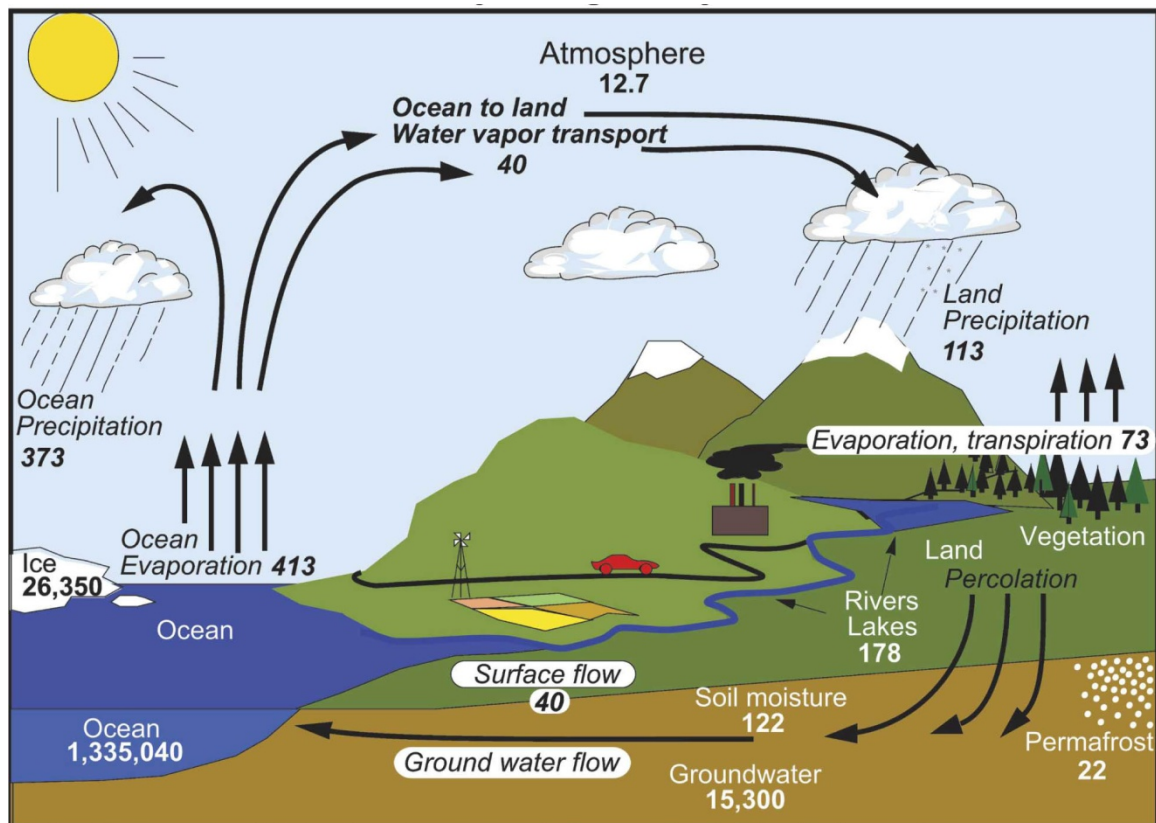
Figure 2.21: The long-term mean global hydrological cycle. Estimates of the main water reservoirs in plain font (e.g. Soil moisture) are given in 10^3 km^3 and estimates of the flows between the reservoirs in italic (e.g. *Surface flow*) are given in 10^3 km^3/year. Figure from Trenberth et al. (2007) who provide information about the sources used to estimate the magnitude of the elements of the cycle and about the uncertainties of the various terms. Copyright 2007 American Meteorological Society (AMS). Reproduced with permission.

A large amount of water is also stored in form of ice, mainly on the Greenland and Antarctic ice sheets (see section 1.4). By contrast, the stock of water in the atmosphere is very low. If the 12.7 10^3 km^3 of atmospheric water estimated in Fig. 2.21 all precipitated, it would correspond to about 2.5 cm of rainfall (=12.7 10^3 km^3/($4\pi R^2$)) over the whole Earth. As the actual precipitation on the Earth's surface is of the order of 1 m per year (see section 1.2), the water in the atmosphere must be being replaced very quickly. This is achieved by evaporation over the ocean and other water bodies as well as by evaporation and transpiration over land. Most of the water that evaporates over the ocean falls back over the ocean (and similarly the water that evaporates over land, falls back over land), but there is also water transfer by the atmosphere from the oceanic area to the land area. This net transfer corresponds to roughly 35% of the total precipitation over land, and is compensated by a surface flow of water (mainly in rivers) from the land to the sea.

According to the **Clausius-Clapeyron equation** (see section 2.1.6), intense evaporation occurs in the warm equatorial areas and in the tropics. In equatorial areas, because of the convergence at the surface and upward motions (see section 1.2), the moist air at low levels rises, reaching colder level. This induces condensation, the formation of clouds and high precipitation rates (see Fig. 1.7). Despite the high temperature and high evaporation rate, equatorial regions thus have more precipitation than evaporation at the

surface (negative *E-P*, Fig. 2.22). In the subtropics, evaporation minus precipitation (*E-P*) is clearly positive, because of the general **subsidence** at these latitudes. At mid to high latitudes, *E-P* is again negative on **zonal** average because of the net moisture transport from tropical areas.
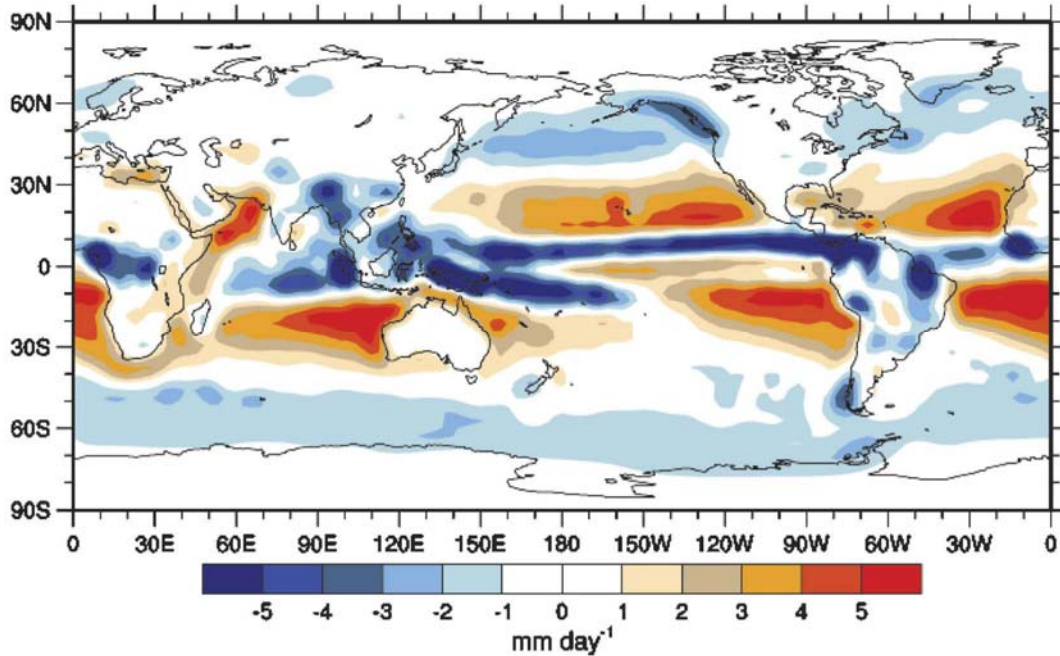

Figure 2.22: Long term annual mean evaporation minus precipitation (*E-P*) budget based on ERA-40 **reanalyses**. Units are mm per day. The major features of the *E-P* budget are represented on this figure, but because of large uncertainties, the values displayed should not be considered as quantitatively correct. There are also some clear discrepancies over land, in particular where net positive evaporation is shown (negative values should generally occur over land as river runoff is positive). Figure from Trenberth et al. (2007). Copyright 2007 American Meteorological Society (AMS), Reproduced with permission.

The imbalance of the water budget over land is generally small and is compensated by river runoff R_{riv} (in the long term mean, R_{riv} nearly equals P-E) which returns water to the sea. Because of the land topography, this river runoff is an important element of the water balance for some ocean basins. For instance, the Arctic Ocean receives about 10% of the total river runoff (mainly from the Russian rivers) although it only constitutes about 3% of the World Ocean. This partly explains why surface water in the Arctic is relatively fresh (see Fig. 1.11).

Over the oceans, the imbalance of the water budget at the surface is larger than over land because it can be compensated for by a net oceanic water transport that is much more efficient (and much larger) than that associated with river runoff. This net oceanic transport counter-balances the large atmospheric moisture transport out of the subtropics towards the equatorial regions and mid and high latitudes. In a way, the net meridional water transport and the associated energy transport in the atmosphere are only possible because the ocean transport is able to compensate for the imbalance at the surface due to the *E-P* fluxes.

Net oceanic water transport can also counterbalance the **zonal** transport by the atmosphere. In particular, because of high *E-P* rates, the Atlantic Ocean is a net evaporative basin and is thus more saline at the surface than the Pacific where the E-P

balance integrated over the whole basin is negative (see Fig. 1.11). As a consequence, the global oceanic circulation must induce a net water transport from the Pacific to the Atlantic to achieve a water balance in both basins.
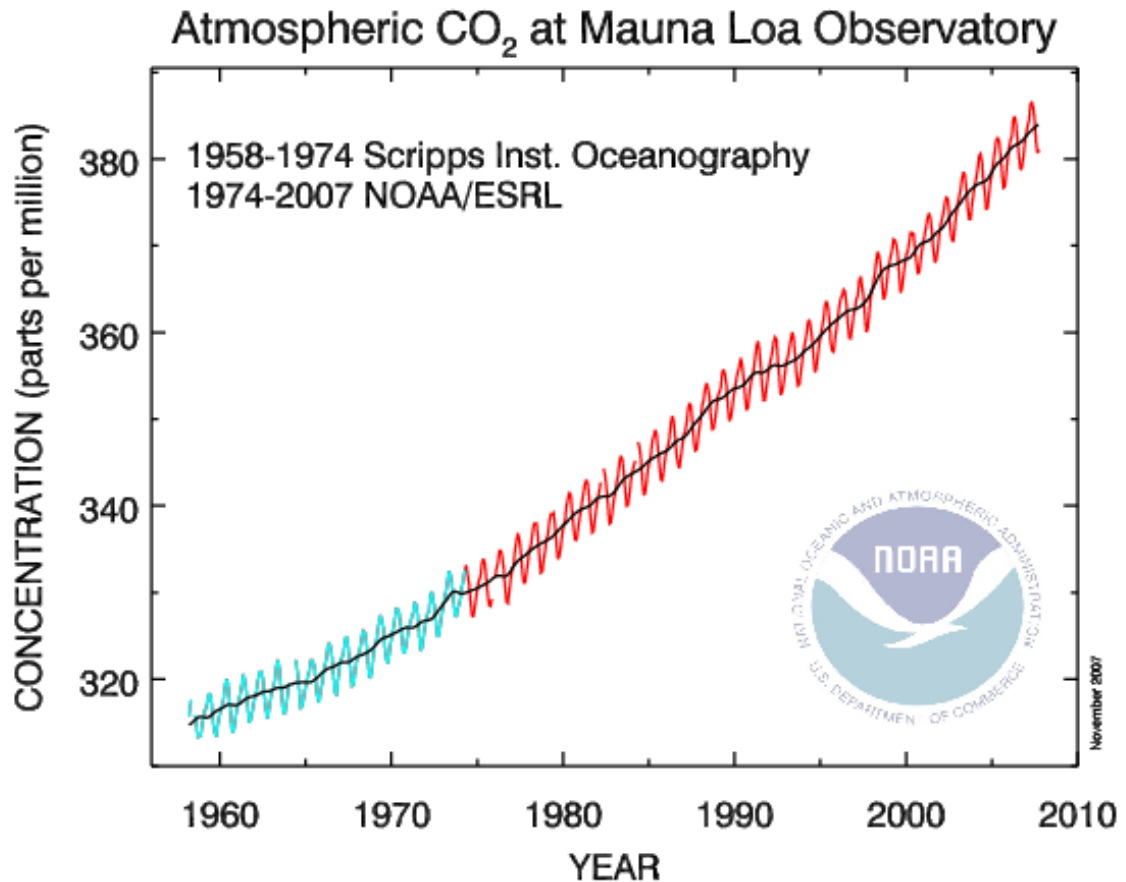

Figure 2.23: Monthly mean atmospheric carbon dioxide at Mauna Loa Observatory, Hawaii (in ppm). The observation were started by C. David Keeling of the Scripps Institution of Oceanography in March of 1958 (blue). The National Oceanic and Atmospheric Administration started its own CO_2 measurements in May of 1974 (red). The black curve represents the seasonally corrected data smoothed with a 6-month window. Source: Dr. Pieter Tans, NOAA/ESRL (www.esrl.noaa.gov/gmd/ccgg/trends/co2_data_flux_rev1.html). Following the policy of U.S. government agencies, this figure is not subject to copyright protection.

2.3 The carbon cycle

2.3.1 Overview

The transfers between the different components of the climate system imply exchanges of heat (section 2.1), exchanges of single molecules such as water (H_2O) with phase changes (section 2.2), and exchanges involving chemical transformations. This latter type of exchange may involve elements such as oxygen, nitrogen, phosphate and sulphur, but one of the most important cycles from a climatic point of view is the carbon cycle because it involves changes in the atmospheric concentration of two important greenhouse gases (section 2.1.2): carbon dioxide (CO_2) and methane (CH_4).

One of the major changes brought about by human activity is the large increase in the atmospheric concentration of those two gases (see Chapter 6). The concentration of carbon dioxide has increased from around 280 ppm in 1800 to 384 ppm in 2007. Because CO_2 is relatively stable, it is well mixed and its concentration in the atmosphere is nearly homogenous away from zones where strong exchanges with the biosphere occur. Those exchanges with the biosphere are also responsible for the weak seasonal cycle observed in the long Mauna Loa record (Fig. 2.23).

CH_4 is more reactive than CO_2 and can be oxidised to form CO_2 and H_2O.

$$CH_4 + 2O_2 \rightarrow CO_2 + 2H_2O \tag{2.37}$$

Its concentration is lower than that of CO_2, but it has increased from 725 ppb to 1780 ppb in 150 years. Methane is naturally produced by the anaerobic breakdown of organic matter in lakes and swamps. Methane is also released into the atmosphere by human activities such as mining, biomass burning and gas production, as well as the production of rice and by ruminants which produce methane as they digest grass.

The atmosphere is a relatively small reservoir of carbon compared to the sedimentary rocks, the ocean and the terrestrial biosphere (which includes non living organic material such as soil carbon) (Fig. 2.24). In particular, more than $50 \cdot 10^6$ GtC (gigatons of carbon or equivalently PgC, petagrams of carbon) are stored in the Earth's crust. This is more than 1000 times the stock in the ocean, more 20 000 times the stock in soil and more than 50 000 times the stock in the atmosphere. However, the changes in the carbon concentration in sedimentary rocks are very small, and the associated fluxes are much lower than those between the ocean, the atmosphere and the soil.
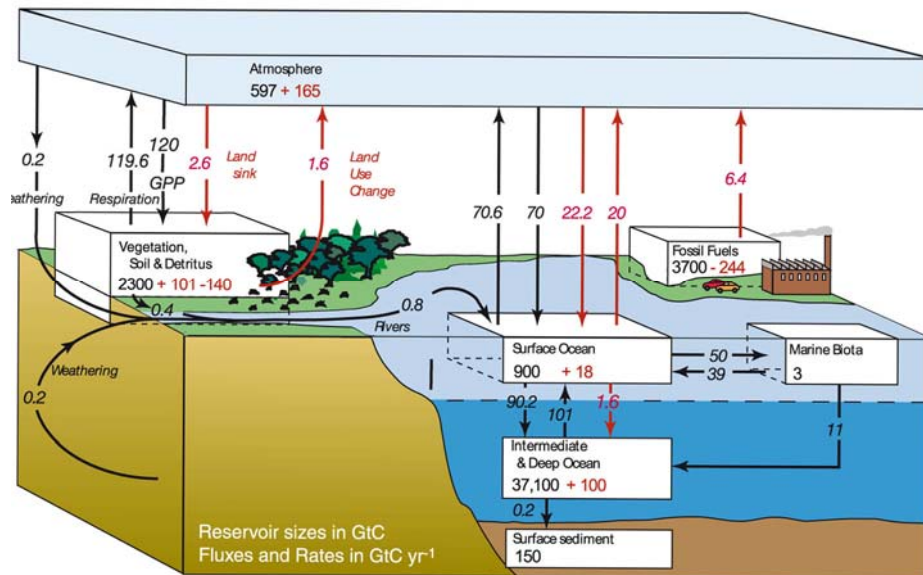
Figure 2.24: The global carbon cycle for the 1990s, showing the main annual fluxes in GtC yr^{-1}: pre-industrial 'natural' fluxes are shown in black and 'anthropogenic' fluxes in red. The carbon stored in deep sediments and in the Earth's crust is estimated at around $50 \cdot 10^6$ GtC. Figure 7.3 from Denman et al. (2007) using a modified legend, published in:Climate Change 2006: The Physical Science Basis. Contribution of Working Group I to the Fourth Assessment Report of the Intergovernmental Panel on Climate Change, Cambridge University Press, copyright IPCC 2007. Reproduced with permission.

Before the industrial era (i.e. before 1750), the exchanges between the various reservoirs were close to equilibrium. However because of anthropogenic carbon release mainly related to fossil-fuel burning and changes in land use (deforestation and agriculture processes), the flux of carbon into the atmosphere has increased dramatically during the last 150 years. Roughly 45% of the anthropogenic carbon released up to now has remained in the atmosphere, which explains the observed rise in atmospheric CO_2. The remaining fraction has been absorbed by the ocean (around 30%) or the terrestrial biosphere (around 25%).

2.3.2 Oceanic carbon cycle

A flux of CO_2 between the ocean and the atmosphere occurs when the CO_2 content of the ocean surface is not in equilibrium with the atmospheric concentration. The flux Φ^{CO_2} from the ocean to the atmosphere is proportional to this imbalance and can be computed as a function of the difference in partial pressure p^{CO_2} between the two media:

$$\Phi^{CO_2} = k^{CO_2} \left(p_W^{CO_2} - p_A^{CO_2} \right) \tag{2.38}$$

where the subscripts A and W refer to air and water, respectively. k^{CO_2} is a transfer coefficient which is strongly dependent on the wind velocity. At equilibrium, $p_W^{CO_2}$ is obviously equal to $p_A^{CO_2}$.
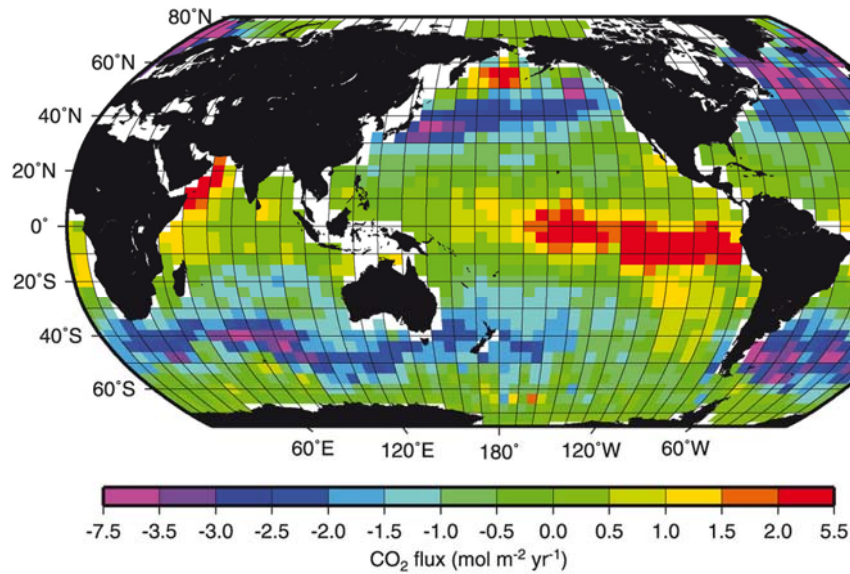
Figure 2.25: Estimates of sea-to-air flux of CO_2. Figure 7.8 from Denman et al. (2007), based on the work of T. Takahashi, available at http://www.ldeo.columbia.edu/res/pi/CO2/carbondioxide/pages/air_sea_flux_rev1. html), using a modified legend, published in: Climate Change 2007: The Physical Science Basis. Contribution of Working Group I to the Fourth Assessment Report of the Intergovernmental Panel on Climate Change, Cambridge University Press, copyright IPCC 2007. Reproduced with permission.

As the surface CO_2 concentration in the atmosphere is nearly homogenous, the repartition of the flux mainly depends on the oceanic p^{CO_2}. Supersaturated zones, where the partial pressure of CO_2 in sea water is higher than in the air, have a positive flux from the ocean to the atmosphere. In present-day conditions, this occurs in tropical regions, particularly in the eastern equatorial Pacific (Fig. 2.25). On the other hand, undersaturated areas, such as the mid to high latitudes around 40°-60° in both hemispheres (except the Northern Pacific), display CO_2 fluxes from the atmosphere to the ocean, i.e. an uptake of CO_2 from the atmosphere.

2.3.2.1 Inorganic carbon cycle

When gaseous CO_2 is transferred from the atmosphere to the ocean, it immediately reacts with water to form carbonic acid (H_2CO_3) which dissociates, leading to the formation of bicarbonate (HCO_3^-) and carbonate ions (CO_3^{2-}):

$$CO_{2(gas)} + H_2O \rightleftharpoons H_2CO_3 \tag{2.39}$$

$$H_2CO_3 \rightleftharpoons H^+ + HCO_3^- \tag{2.40}$$

$$HCO_3^- \rightleftharpoons H^+ + CO_3^{2-} \tag{2.41}$$

The sum of these three forms of carbon is often referred to as Dissolved Inorganic Carbon (**DIC**):

$$DIC = \left[H_2CO_3\right] + \left[HCO_3^-\right] + \left[CO_3^{2-}\right] \tag{2.42}$$

The reactions (2.39 to 2.41) are so fast that, to a good approximation, the three components are always in equilibrium. The equilibrium relationship between the different molecules involved in reaction (2.39) can then be used to define the **solubility** K_H of CO_2, which relates the concentration of carbonic acid to the partial pressure of carbon dioxide (pCO_2).

$$K_H = \frac{\left[H_2CO_3\right]}{pCO_2} \tag{2.43}$$

By definition, for the same atmospheric pCO_2, the amount of carbonic acid in the ocean at equilibrium will be larger for a high solubility than for a low solubility. The transfer of CO_2 between the ocean and the atmosphere (Eq. 2.38) can then easily be expressed as a function of $[H_2CO_3]$ using (Eq. 2.43).

In the sea, the equilibrium between the different forms of carbon occurs when nearly 90% of the dissolved inorganic carbon is in the form of bicarbonate, around 10% is carbonate, and only 0.5% is carbonic acid. This predominance of carbonate and bicarbonate ions explains why the ocean is able to store much more carbon than the atmosphere, while it is not true for other gases (such as oxygen) which have similar solubility to CO_2. Furthermore, reactions (2.39 to 2.41) show that atmospheric CO_2 must balance the whole pool of DIC, not just H_2CO_3. As DIC is dominated by HCO_3^- and

CO_3^{2-}, the atmosphere-ocean exchanges will be strongly influenced by the concentration in these ions. For instance, it has been estimated that only 1 molecule in 20 of the CO_2 entering the ocean stays as H_2CO_3, the large majority reacting with CO_3^{2-} to form HCO_3^-, the dominant species in *DIC*:

$$H_2CO_3 + CO_3^{2-} \rightleftharpoons 2HCO_3^- \tag{2.44}$$

The ocean-atmosphere fluxes are thus strongly influenced by the availability of CO_3^{2-}. Additionally, because of the small fraction of incoming CO_2 staying as H_2CO_3 and thus influencing the p^{CO_2} in the ocean, the time taken to reach equilibrium between the ocean and the atmosphere is about 6 months - around 20 times longer than if this reaction were not active.

As shown in reactions (2.40 and 2.41), the dissociation of H_2CO_3 causes the water to become more acidic. This effect is commonly measured through the alkalinity *Alk*, defined as the excess of bases over acid in water:

$$Alk = \left[HCO_3^-\right] + 2\left[CO_3^{2-}\right] + \left[OH^-\right] - \left[H^+\right] + \left[B(OH)_4^-\right] + \text{minor bases} \tag{2.45}$$

where $\left[B(OH)_4^-\right]$ is the borate ion. The total alkalinity is dominated by the influence of bicarbonate and carbonate ions, meaning that a tight link exists between *Alk* and the concentration of the three forms of carbon. Conversely, changes in total alkalinity or in the acidity of the ocean can have a strong influence on the equilibrium of the reactions (2.40 and 2.41). For instance, if *Alk* decreases (or equivalently if the system become more acid), the equilibrium of reactions (2.40) and (2.41) will be pushed toward the formation of more H_2CO_3 and HCO_3^-, increasing the concentration of H_2CO_3 and thus the p^{CO_2} with a potential influence on air-sea fluxes. The estimates of this effect suggest an increase in 10% of the p^{CO_2} for a 1% decrease in *Alk*.

On the basis of this discussion, we can return to Fig. 2.25 and try to explain the distribution of the air-sea fluxes of CO_2. The solubility of CO_2, or equivalently the equilibrium constant of reaction (2.39) is strongly dependent on temperature. A water parcel that is cooled, as it flows northward for instance, will take up atmospheric CO_2, while a water parcel that is warmed will release CO_2 to the atmosphere. This generally leads to positive ocean-atmosphere fluxes in tropical regions and negative ones at high latitudes, as shown in Fig. 2.25.

2.3.2.2 Biological pumps

In addition to the purely thermal effect, biological processes also play a significant role in the distribution of surface fluxes of CO_2 by affecting *DIC* and *Alk*. A first important reaction is the photosynthesis in which phytoplankton uses solar radiation to form organic matter from CO_2 and water:

$$6CO_2 + 6H_2O \rightleftharpoons C_6H_{12}O_6 + 6O_2 \tag{2.46}$$
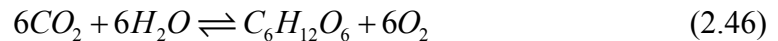
Conversely, organic matter can be dissociated to form inorganic carbon (the reverse process of photosynthesis) by respiration and remineralisation of dead phytoplankton and detritus.

Reaction 2.46 is a highly simplified representation of the complex biological processes associated with photosynthesis. In particular, it hides the fact that, in order to produce organic matter, phytoplankton need nutrients (mainly nitrates and phosphates) as well as minor elements such as iron. As those nutrients generally have low concentrations in surface water where light is available for photosynthesis, their concentration is often the limiting factor for biological production.

Because particles whose density is more than that of water settle out, and some particles are transported by ocean currents, a fraction of the organic matter is exported downward out of the surface layer. The net downward flux of carbon associated with this transport of organic matter is called the **soft tissue pump**. A significant part of the remineralisation thus occurs in the deep layers where it produces an increase in *DIC* and the release of nutrients. The deep waters are thus rich in nutrients. Where they **upwell** toward the surface, the surface concentration of nutrients increases, generally leading to high biological production, such as that observed off the coasts of Peru and Mauritania.

A second important biological process is related to the production of calcium carbonate (in form of **calcite** or **aragonite**) by different species, in particular to form their shells:

$$Ca^{2+} + CO_3^{2-} \rightleftharpoons CaCO_3 \qquad (2.47)$$

This production influences both the *DIC* and the *Alk* and can thus have a large influence on the carbon cycle. For instance, $CaCO_3$ production implies a reduction in *Alk* (see Eq. 2.45), which in turns lead to an increase in oceanic p^{CO_2} and reduces the uptake of atmospheric CO_2 by the ocean. An alternative way to view this mechanism is to say that $CaCO_3$ production reduces the concentration of CO_3^{2-} in the ocean and thus the availability of this ion to combine with H_2CO_3 to produce HCO_3^- (reaction 2.44), so increasing $[H_2CO_3]$ and p^{CO_2}.

The dissolution of calcite and aragonite mainly occurs at great depth (see section 4.3.1), following the precipitation of particles and dead organisms. This leads to the *Alk* and *DIC* being transported downwards, a system called the **carbonate pump**. A third pump, called the **solubility pump**, is associated with the sinking of cold surface water, characterised by a relatively high solubility of CO_2 and thus high *DIC,* to great depths at high latitudes. All these downward transports have to be compensated for at equilibrium by an upward flux of inorganic carbon by the oceanic circulation.

Because of the three pumps briefly described above, DIC is about 15% higher at depths than at the surface. The soft tissue pump plays the largest role in the observed vertical gradient. This distribution has a profound influence on the atmospheric CO_2 concentration. Indeed, if *DIC* were perfectly homogenous in the water column (i.e. had higher surface values and lower depth values than currently observed), the concentration of atmospheric CO_2 would be much higher. More realistically, when deep water upwells to the surface, CO_2 will tend to escape from the ocean because of the high *DIC*. However, as the deep waters are rich in nutrients, the biological uptake associated with photosynthesis can compensate for the influence of a higher *DIC*. The net effect depends on the regions, generally resulting in positive ocean-atmosphere CO_2 fluxes at high

latitudes and negative ones at low latitudes, partly offsetting the direct temperature effect (Fig. 2.25).

2.3.3 Terrestrial carbon cycle

The uptake of carbon through photosynthesis by land plants is larger than the corresponding uptake by phytoplankton, in particular in spring because of the greening of forest at mid and high latitudes and of the growth of herbaceous plants (Fig. 2.26). About half of this primary production is directly transferred back to the atmosphere by the respiration of the land plants themselves, the remaining part being incorporated into leaves, woods and roots (this fraction is defined as the **net primary production, NPP**).
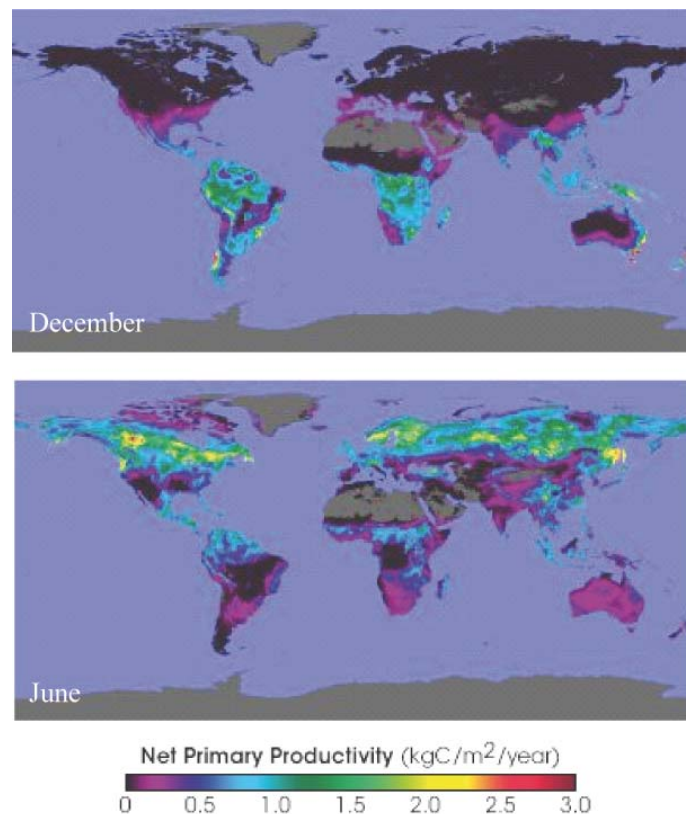

Figrue 2.26: Net productivity over land in December 2004 and June 2005. *Source*: NASA Earth Observatory, http://earthobservatory.nasa.gov/. Following the policy of U.S. government agencies, this figure is not subject to copyright protection.

The large majority of the carbon fixed by NPP returns to the atmosphere through decomposition in soil, the respiration of herbivores and carnivores, and fire. However, the time needed for this transfer back to the atmosphere is related to a large number of relatively complex processes. For instance, the carbon is stored for much longer in trees than in leaves or grasses. When plants die or leaves fall on the ground and enter the pool of organic matter in the soil, the decomposition rate depends strongly on the chemical composition of the organic material, the temperature and humidity of the soil, etc. Some of the organic matter in the soil is quickly remineralised, but much of it remains in the soil pool for decades or longer.

2.3.4 Geological reservoirs

The majority of the organic carbon that is exported downward from the surface layer is remineralised in the water column. In particular, the ocean is undersaturated with respect to calcite (aragonite) below 4500m (3000m) in the Atlantic and below 800 m (600m) in the Pacific. As a consequence, the long-term burial of $CaCO_3$ in the sediments to produce **limestone** mainly occurs in shallow seas (for instance in coral reefs). Averaged over the whole ocean, this long term burial corresponds to 13% of the export of $CaCO_3$ out of the surface layer. On short **timescales**, this is a small fraction of the whole carbon cycle, but it becomes a crucial component on timescales longer than a century. An even smaller percentage of the organic carbon is stored in the form of natural gas, oil and coal.

Because the sea floor spreads due to plate tectonics, sediments are transported horizontally and are eventually incorporated within the mantle through **subduction** along plate boundaries. At higher temperatures and pressure, limestone is transformed during **subduction** into calcium-silicate rocks (this is called **metamorphism**) by the reaction:

$$CaCO_3 + SiO_2 \rightarrow CaSiO_3 + CO_2 \qquad (2.48)$$

The CO_2 that is released in this reaction can return to the atmosphere, in particular through volcanic eruptions.

The plate motion also allows the calcium-silicate rocks to be uplifted to the continental surface, where they are affected by physical and chemical **weathering**. In particular, the carbonic acid contained in rain water (in the same process as reaction 2.39) can interact with the calcium-silicate rocks:

$$CaSiO_3 + H_2CO_3 \rightarrow CaCO_3 + SiO_2 + H_2O \qquad (2.49)$$
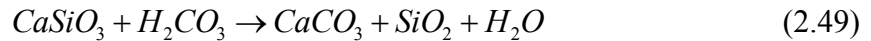
The products of this reaction are transported by rivers to the sea where they can compensate for the net export of $CaCO_3$ by sedimentation. Weathering thus tends to reduce atmospheric CO_2 by taking up carbonic acid to make $CaCO_3$ and increasing ocean alkalinity while metamorphism and sedimentation tend to increase atmospheric CO_2. Overall sedimentation, subduction and metamorphism, and weathering form a closed loop that takes place over millions of years, and is sometimes referred to as the long term inorganic carbon cycle (Fig. 2.27).
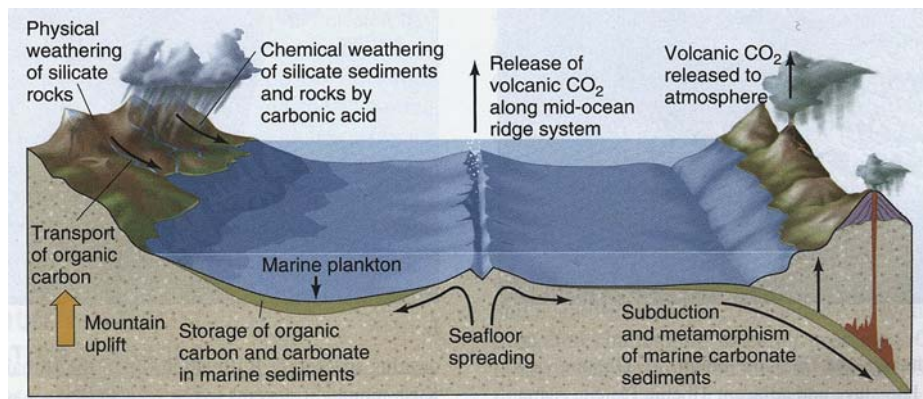

Figure 2.27: Long term inorganic carbon cycle through sedimentation, subduction and metamorphism, and weathering. Figure from Skinner et al. (2004). Copyright 2004 John Wiley & Sons, Inc. Reproduced with permission.

Cited references and further reading

Adams J. (2007). Vegetation-climate interaction. How vegetation makes the global environment. Springer in association with Praxis Publishing, Chichester, UK, 232pp.

Curry J.A. and P.J. Webster (1999). Thermodynamics of atmosphere and oceans. International Geophysics series, volume 65. Academic Press, 468 pp.

Denman, K.L., G. Brasseur, A. Chidthaisong, P. Ciais, P.M. Cox, R.E. Dickinson, D. Hauglustaine, C. Heinze, E. Holland, D. Jacob, U. Lohmann, S Ramachandran, P.L. da Silva Dias, S.C. Wofsy and X. Zhang (2007). Couplings Between Changes in the Climate System and Biogeochemistry. In: *Climate Change 2007: The Physical Science Basis. Contribution of Working Group I to the Fourth Assessment Report of the Intergovernmental Panel on Climate Change.* Solomon, S., D. Qin, M. Manning, Z. Chen, M. Marquis, K.B. Averyt, M.Tignor and H.L. Miller (Eds.). Cambridge University Press, Cambridge, United Kingdom and New York, NY, USA.

Fasullo, J. T., and K. E. Trenberth, 2008: The annual cycle of the energy budget. Part II: Meridional structures and poleward transports. J. Climate 21: 2313-2325.

Hartmann D.L. (1994). Global physical climatology. International Geophysics series, volume 56. Academic Press, 412 pp.

IPCC (2007). *Climate Change 2007: The Physical Basis. Contribution of Working Group I to the Fourth Assessment Report of the Intergovernmental Panel on Climate Change.* Solomon, S., Qin, D., Manning, M., Chen, Z., Marquis, M., Averyt, K.B., Tignor, M., and Miller H.L. (Eds.). Cambridge University Press, Cambridge, United Kingdom and New York, NY, USA, 996 pp.

Kalnay, E. and 21 others (1996). The NCEP/NCAR 40-year reanalysis project. Bulletin of the American Meteorological Society 77: 437-471.

Kiehl J. and K. Trenberth (1997). Earth's annual global mean energy budget. Bulletin of the American Meteorological Society 78: 197-2006.

Marshall J. and R.A. Plumb (2007). Atmosphere, ocean and climate dynamics: an introductory text. International Geophysics, volume 93. Academic Press, 344 pp.

Millero F.J. (2005). Chemical oceanography (third edition). Taylor and Francis, 496pp.

Rayner N.A., D.E. Parker, E.B. Horton, C.K. Folland, L.V. Alexander, D.P. Rowell, E.C. Kent and A. Kaplan (2003). Global analyses of sea surface temperature, sea ice, and nigh marine aire temperature since the late nineteenth century. Journal of Geophysical Research 108 (D14): 4407, doi:10.1029/2002JD002670.

Sarmiento G.L and N. Gruber (2006). Ocean biogeochemical dynamics. Princeton University Press, 503pp.

Skinner B.J., S.C. Porter and J. Park (2004). Dynamic Earth, an introduction to physical geology, fifth edition. Wiley, 584pp.

Taylor F.W. (2005). Elementary Climate Physics. Oxford University Press. 212pp

Trenberth K.E. and J.M. Caron, (2001). Estimates of meridional atmosphere and ocean heat transport. Journal of Climate 14: 3433-3443.

Trenberth, K. E. and D. P. Stepaniak (2003). Seamless poleward atmospheric energy transports and implications for the Hadley circulation. J. Climate 16: 3705-3721.

Trenberth K.E., L. Smith, T.T. Qian , A.G. Dai and J. Fasullo (2007). Estimates of the global water budget and its annual cycle using observational and model data. Journal of Hydrometeorology 8 (4): 758-769.

Trenberth, K. E., J. T. Fasullo and J. Kiehl (2009). Earth's global energy budget. Bull. Amer. Meteor. Soc., 90: 311-323.

Wallace J.M. and P.V. Hobbs (2006). Atmospheric science: an introductory survey (2nd edition). International Geophysics Series 92, Associated press, 484pp.

Exercises

1. Using a model similar to the one described in section 2.1.2, derive the relation between T_e and T_s for an arbitrary number n of atmospheric layers in radiative equilibrium, each having an emissivity of 1.
2. Using the information provided in section 2.1.3, compute the length of the various seasons.
3. Demonstrate Eq. 2.19.
4. Compute the temperature that would occur at the pole and the equator if the incoming radiation were the same as presently observed on Earth but there was no heat transport.
5. On the basis of the transport of water by the thermohaline circulation and of the temperature of the different water masses, estimate the amount of heat transported by the thermohaline circulation.

Additional exercises available on the textbook website (http://www.climate.be/textbook) and on iCampus for registered students.